Analysis of adhesive joints for aerospace applications

Eduardo André de Sousa Marques

Dissertação do MIEM

Orientador: Prof. Lucas F. M. da Silva

Universidade do Porto

Faculdade de Engenharia

FEUP

Faculdade de Engenharia da Universidade do Porto

Mestrado Integrado em Engenharia Mecânica

Fevereiro de 2008

I. RESUMO

Este trabalho foca-se em tecnologias e técnicas de adesão destinadas ao uso em aplicações de alta temperatura. Muitas indústrias exigem ligações leves, fortes e resistentes à temperatura nas quais estas técnicas podem ser aplicadas. Para atingir as resistências necessárias a alta temperatura várias soluções foram estudadas. Adesivos cerâmicos, silicone de alta temperatura (RTV) e combinação de dois adesivos foram algumas das técnicas consideradas.

A caracterização de adesivos cerâmicos é um dos principais pontos do trabalho experimental, disponibilizando as propriedades mecânicas de um destes adesivos de modo a que simulações possam ser implementadas. As técnicas de aplicação prática destes adesivos foram também estudadas, uma vez que estes materiais se comportam de modo muito diferente dos mais comuns adesivos poliméricos e como tal podem requerer ferramentas e procedimentos específicos.

Os silicones com ponto de vulcanização à temperatura ambiente (Room Temperature Vulcanizing – RTV's) são também objecto de estudo. Estes são actualmente utilizados na indústria aeroespacial em aplicações de alta temperatura e como tal são um ponto de partida lógico no desenvolvimento de ligações adesivas de alta temperatura.

O uso de adesivos duplos é também um ponto focal importante, dado que trabalho experimental prévio já demonstrou que a combinação de adesivos com propriedades mecânicas dramaticamente diferentes pode ser projectado para obter juntas com resistências mecânicas muito boas.

II. ABSTRACT

The adhesion technologies and procedures studied in this work are focused on the requirement of high temperature resistance. Many industries require lightweight, strong and heat resisting connections in which these techniques can be employed.

To achieve the necessary resistance at high temperature, various possibilities were studied. Ceramic adhesives, high temperature silicones (RTV) and dual adhesive use are all considered.

The characterization of a ceramic adhesive is one of the main points of the experimental work, making its mechanical properties available so that they can be used in simulation work. The practical application techniques for these adhesives is also studied as these material behave very differently from the common polymeric adhesives and may require specially designed tooling and procedures.

Silicones with room temperature vulcanizing (RTV's) are also object of study. These are currently used in the aerospace industry in high temperature applications, and as such are a logical starting point for the development of high temperature adhesive connections.

The use of adhesive combinations is also a main focus point, as previous experimental work has demonstrated that the combination of adhesives with dramatically different mechanical properties can be projected to obtain joints with very good mechanical resistance.

III. ACKNOWLEDGEMENTS

Dr Lucas F.M. da Silva

Mr Joaquim Fonseca

Mr Miguel Figueiredo

Mr Raul Campilho

Mr Filipe Chaves

Ms Mariana Banea

Mr Rui Silva

Mrs Emilia Soares

Mr Hélder Ferreira

IV. INDEX

V. FIGURE INDEX

VI. TABLE INDEX

1. INTRODUCTION

Adhesive connections are currently widely accepted as an extremely valuable tool in mechanical design, allowing the production of connections with a very good strength-to-weight ratio. Aerospace, automotive and railway industries are among those that use adhesive techniques extensively, gaining benefits from the ability to join various different materials and the relatively simple manufacturing process, while keeping the weight down. While the nature of adhesive connections does not allow it to replace all other connection techniques, a judicious use of it and the correct combination with other connection techniques can result in synergies that benefit the final product.

With all these advantages, it is only natural that the field of application of adhesive techniques is being constantly expanded, bringing new solutions to some older problems. High temperature connection technique is one of these problems. This is a very complex problem that the aerospace industry faces. In this application, many joints face extremely large temperature ranges, which derive from the high altitudes and high speeds encountered. As always in this industry, the connections must be as light as possible and extremely predictable and reliable. Adhesive joints are definitely a major candidate for these requirements.

There are a few techniques currently used to achieve temperature resistant adhesive connections. These are studied and explained in detail in the following chapter. Most of the current solutions used in high performance engineering applications are limited to a maximum of 260ºC (RTV). For the large majority of aeronautical applications regarding atmospheric flight regimen this is more than enough, but, when considering supersonic flight modes and reentry from orbit (common aerospace regimen) one finds than this temperature is insufficient and a large amount of shielding is necessary between the heat source and the adhesive joint. This is especially true in heat shielding applications. With more temperature resistant adhesives, it is arguable that one can design joints nearer to the heat source, resulting in smaller and lighter heat shield packages, with all the usual advantages that come from these characteristics.

Still considering aerospace applications, it must be remembered, though, that high temperatures are only a transient part of the flight regimen. While in space, the joint will not be subjected to high temperatures but to the low, freezing temperatures of space. The temperatures will be as low as -156 Cº. While the strength requirements at this phase will not be on par with the requirements at high temperature, the joint still must provide some degree of resistance at these temperatures

This brings us to the main objective of this work, which is the development of a dual adhesive, combining two different adhesives, with radically different mechanical properties. Combination of adhesives has been previously demonstrated as a possible method to improve the behavior of the joint in high temperature loadings. In this specific case the combination of adhesives will also be used to support the connection at low temperature levels.

To achieve this purpose, the dual adhesive joint must be composed of two different adhesives with completely different mechanical properties. One adhesive works as the high temperature adhesive (abbreviated HTA), providing load transfer in these conditions. This adhesive must not fail when the joint is at low temperatures so that it can sustain the load when the joint is used again at high temperatures. The other adhesive is called the low temperature adhesive (LTA) and must be able to provide satisfactory connection at low temperatures. It must be a ductile adhesive and must not degrade with the cyclic progression from low to high temperatures that the joint is expected to withstand.

The degradation of the low temperature adhesive at the high temperatures is a major technical challenge of this approach. A careful selection of low temperature adhesive and joint geometry is needed to achieve a satisfactory behavior. Another related challenge is the accommodation of thermal stresses in the joint. Cracking of the high temperature adhesive is a strong possibility at the lower end of the temperature spectrum. Detailed geometry considerations must be undertaken, focusing in the distribution of both adhesives in the joint.

A wide range of testing techniques is required to gather the data necessary to validate and help design the bonding procedure. Bulk tensile testing and thick adherent shear testing are the first procedures to be executed, as they provide the basic information about the adhesive mechanical behavior.

A suitable testing technique also has to be developed to simulate most of the loads present in the intended application. While in a first stage only temperature testing is needed, it would be interesting to do some testing in low pressure and high velocity airflow too.

2. HIGH TEMPERATURE ADHESION AND ADHESIVES

2.1 CERAMIC ADHESIVES

Ceramic adhesives are a solution for bonding material with high temperature resistance. Conventional organic adhesives are restricted to temperatures below 300 ºC (bismalemids and polyimides). This makes them unsuitable to bond metals and ceramics that can work continuously at temperatures significantly higher than 300 ºC.

Ceramic adhesives are not organic, so they do not experience combustion or degrade quickly with temperature. Some can operate at temperatures higher than 2000 ºC. The adhesives are based in inorganic binding compounds such as alkali silicates and metal phosphates. Carbon, alumina, silica, magnesia or zirconia powder is commonly used as filler.

The adhesives are usually available in two part systems, in which one of the components is the binder and the other is the filler. Joining these two components results in a slurry that must be quickly applied to the substrate. The assembly must then be cured, which requires temperatures between 260 and 1000 ºC. The different combinations between binder and filler can be optimized to more closely match the coefficient of thermal expansion of the substrate and reduce stresses during heating and cooling phases.

Adhesive ceramics as currently used do not offer a hermetic connection or high degrees of reliability. Their reliability and resistance is below that offered by high performance ceramics, and this can result in cracking under thermal stresses. The use of these adhesives is therefore a very complex proposition and requires careful design.

A joint bonded with ceramic adhesives can be inspected and tested using scanning electron microscopy, mechanical testing and thermal imaging.

The use of two adhesives with different thermal behavior combined can result in joints with exceptional properties. It has been demonstrated that according to the mixed modulus concept, at high temperatures a brittle adhesive (with high modulus) will retain its strength and hold the joint together (1). At low temperatures, a ductile adhesive takes over and supports the majority of the load. The resulting joint will be able to sustain more load than a high temperature adhesive alone at the lowest temperatures or a low temperature adhesive at the higher temperatures. Experimental work performed with polymeric adhesives also demonstrates that the resistance of the joint at high temperatures is somewhat inferior to the resistance of the high temperature adhesive. A similar effect is seen at the lowest temperatures (2). The choice of polymeric adhesives is particularly important as they must exhibit resistance to degradation after a series of cycles at high temperature. Concerning the geometry of the connection, most of the studies focus in single lap joints. In these joints the ductile adhesive is introduced in the extremities (where there is more deformation and peel stresses) while the stiffer and more brittle adhesive is placed in the center of the joint, where it is safeguarded from excessive deformation.

Ceramic materials have been combined with high temperature organic adhesives to provide additional temperature resistance. Tests done with formaldehyde resin and ceramic fillers have identified some of the factors responsible for this effect (3). The first effect is the substitution of a large volume of volatile material for ceramic material. The second effect is additional oxidation of the ceramic materials induced by the release of oxygen during the decomposition of the resin matrix. The oxidation expands the ceramic component and allows the migration of some ceramics with low point of fusion into the zones subjected to heat, effectively replacing the resin in those areas. The resin is used to provide strength in low temperatures and as a matrix to hold the ceramics components. Once high temperatures are achieved, the resin matrix loses resistance and the ceramic adhesives assume the bulk of the connection strength.

2.2 CERAMIC-CERAMIC ADHESION

Ceramic-ceramic joints were experimentally observed to be susceptible to two different modes of failure: failure at the adhesive-adherend interface or cohesive failure of the adhesive joint (with failure propagation entirely in the adhesive bulk or partially at the adhesive-adherend interface (4). The ability of a ceramic adhesive to correctly wet the joint and spread in the available area is very dependent on the viscosity of the adhesive (5). Very viscous adhesives exhibit reduced bonding strength. Low coefficients of thermal expansion are also very important: when comparing two adhesives with approximately the same mechanical properties except the coefficient of thermal expansion it was found that the adhesive with the lowest CTE provides the highest mechanical resistance.

2.3 METAL-CERAMIC ADHESION

Metal-ceramic adhesion is an area that has seen considerable scientific study. This is due to the importance and remarkable capabilities of such connections in certain engineering applications. Aerospace companies are some of the main users of these joints but there also other areas of manufacturing that require high temperature connections between ceramic and metal. Furnaces, ovens and high temperature instrumentation are the main areas.

Detailed chemical studies of metal-ceramic joints demonstrate that the purity of the interface is a very important parameter for the absolute resistance of the connection. Impurities are usually responsible for a decrease in adhesive energies. There are however exceptions, such as the presence of carbon in an MgO-Al interface layer. In this configuration there is up to 61% increase in the adhesion energies (6).

Impurities can also modify the peak stresses verified in the interface. In the example presented above, carbon induces greater peak stresses while presence of sulfur reduces them by a factor of two. This demonstrates the importance of controlling the elements present in the joint during manufacturing.

Metal-ceramic connections show a combination of different chemical bonding types: some of the bond regions exhibit pairs of positive and negatively charged particles along the interface, creating ionic connections; metallic/covalent connections make up the rest of the connections observed along the interface(6).

Connections between metal and ceramic therefore always require a good surface preparation, particularly the introduction of an oxide layer in the surface, promoting covalent bonding.

Bhowmik et al (7) tested the influence of the surface treatment in a series of experiments designed to represent the demands of a space application. Titanium adherends were bonded in a single lap joint configuration with Cotronics Resbond 907GF (Brooklyn, New York, United States of America) ceramic adhesive. Some specimens were subjected to a careful brushing and anodizing surface treatment while others were left untreated. The specimens were tested in three different situations. The first of these was an aggressive chemical environment using a very effective chemical solution called Ringer's solution. It was found that the anodized surfaces kept their normal strength even when immersed in this aggressive solution. The next test was a radiation exposure test. The samples were subjected to a 37 kGy/h radiation dose in the neutron moderator pool of a nuclear reactor. There was no discernible loss of strength under these conditions, so it was concluded that ceramic adhesives are impervious to high radiation environments. Lastly, joints were tested at 500ºC and -80ºC. There was a small loss of strength for both cases, but the joint displayed remarkably consistent resistance at both temperatures, demonstrating the excellent thermal properties of ceramic adhesives.

2.4 CERAMIC SURFACE PREPARATION TECHNIQUES

An extensively studied technique for preparation of ceramic surfaces is the Laser Surface Modification. This is a laser ablation process that modifies the surface of material creating micro-columns of projected material, improving the strength of a bond performed in that substrate. This improvement is due to several factors (8):

- Increase in the surface area
- Mechanical locking between the adhesive and the micro-columns
- Modification to the surface chemistry/improvements in wettability

The process can be performed either in metals or ceramics. Bond strength improvements were observed in titanium, steel, aluminum, silica Si_3N_4 and TiC substrates.

When the laser energy impacts the substrate surface, some of the material suffers a phase change and it is projected vertically from the heat source, forming a conical column. The resulting morphology is easily visible in a Scanning Electron Microscope, and is depicted in Figure 1(8). By experimenting with different laser settings and observing the resulting surface pattern in ceramics, it was found that the number of conical structures is directly influenced by the laser energy density. Ablation depths are related to the type of ceramics and the processing parameters (9). When using this technique in metals, excessive energy can cause excessive surface melting (10). Also, the resulting surface morphology is not directly related to surface energy as is the case in ceramics. In any case, the maximum shear lap joint was observed in the specimens with the maximum number of conical structures.

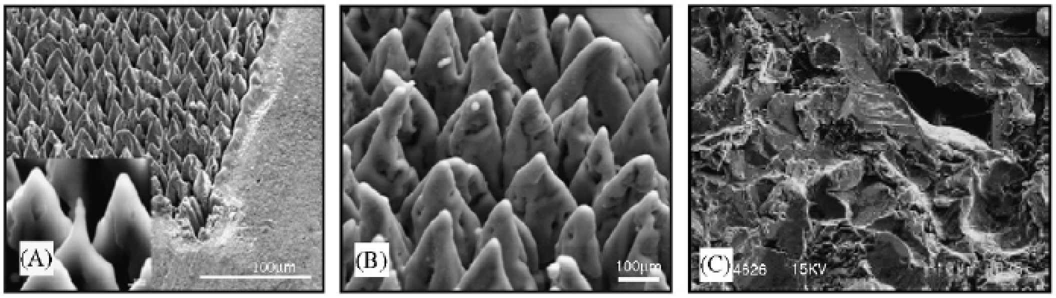

FIGURE 1- SEM IMAGES OF LASER TREATED SURFACE (10)

The chemical effects of the laser treatments can be varied and depend fundamentally of the base material. Silica substrates, for example, when subjected to ultraviolet laser irradiation suffer surface dehydroxylation and change from hydrophilic to hydrophobic. This increases the resistance to contamination of a surface (11). Other ceramic materials can also be formed by additional oxidation during the laser treatment, SiO_2 was observed forming during SiN_4 laser treatment.

The lasers used vary in type and power. The energy needed to melt metal surfaces is 1 J/cm^2 for a laser with a pulse width of 20-50 ns. Some experimental procedures use up to 50 J/cm^2 to promote the formation of plasma above the surface of the metal (12). This plasma cleans the material from contamination. Ceramic treatment is performed energy density around 4 J/cm^2. Some experimental work demonstrates that this energy is the one that creates the maximum number of conical structures. When using the laser just for surface cleaning procedures the energy density is usually orders of magnitude smaller and can be as low as 40 $\mu J/cm^2$(11).

2.5 FUNCTIONALLY GRADED MATERIALS

When mentioning the combination of different materials or adhesives it is necessary to mention the relatively new field of research know as Functionally Graded Materials (FGM). This is a concept that tries to enhance the properties of an object by using and combining the properties and advantages of two different materials. While composites also use the combination of properties of two materials, FGM's introduce gradual material variations, which can take the form of different proportions, ratios or angles of orientation among others (13).

If we consider the specific case of adhesive connections, or more specifically, high temperature joints, we find that this a very interesting approach to solve the problem of providing good resistance at high (1000ºC) and low temperatures (-50ºC or less). If a graded combination of adhesives can be implemented to better accommodate the stress derived from thermal and mechanical loads the resulting joint will surely be stronger. This concept is even more relevant if we consider the combination of adhesives with dramatically different properties.

Specific manufacturing techniques are required for the implementation of this concept. If we consider an adhesive joint we can achieve a gradual variation of properties with some different approaches. A small list of possible techniques is provided below.

2.5.1 Differentiated adhesive cure

A possible solution to use this technique is the use of a different cure process in distinct sections of the joint. A specially formulated adhesive would probably be required, one that would be able to provide different stiffness and/or tensile strength when faced with different curing heat inputs. In two part adhesives (resin + hardener) one could also vary the amount of hardener present in each point of the layer. With careful dosage this would allow a precise control of stiffness. Though interesting, this is not a simple technique to implement and would probably require automated and complex equipment.

2.5.2 Layer thickness variation

This technique is the most easy to implement and consequentially it is used in practical applications. The premise behind this technique is that different layer thicknesses will have different mechanical behavior (14). They can be implemented by use of specially shaped substrates. Layer thickness can also be controlled and optimized to provide economical and lightweight bonding solutions, as the adhesive can be placed only where it is strictly necessary and with the exact thickness to provide adequate stiffness and resistance. Bond thickness variations can also be used to provide adequate fracture toughness to regions of the joint more susceptible to impact damage (15).

2.5.3 Micro adhesive dispensing

Using a micro dispenser system allows a more precise control of the adhesive ratios in each specific location of a joint, which combined with finite element modeling can be optimized to optimal behavior. Automated dispensing techniques have already been used for aerospace applications. It was found that the use of an automated dispensing system can provide better thickness control and prevent the appearance of voids in the adhesive layer.

Direct inkjet printing of adhesives is not only restricted to polymeric material. Simulation and experimental work has demonstrated the viability of this concept for ceramics (16), which suggests the usefulness of this technique for high temperature aerospace applications. Some companies already produce industrial equipment destined to be used in this application. These systems can typically operate at deposition frequencies nearing 100 Hz, provide contactless dispensing in a laminar jet. The volumes applied per discharge are very small, in the order of a few hundreds of nano-liters. The illustration of such a machine is presented in Figure 2.

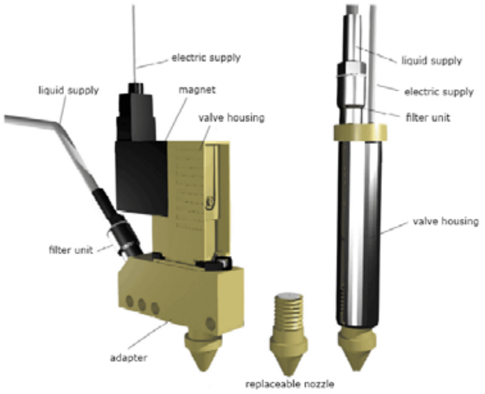

FIGURE 2- NANOJET ADHESIVE DISPENSING SYSTEM (MICRODROP TECHNOLOGIES GMBH)

2.6 JOINT TESTING TECHNIQUES FOR HIGH AND LOW TEMPERATURE

High temperature adhesives raise new difficulties for the already complex testing procedures. There are several techniques available for testing bonds and mechanical joints at the lowest and highest temperatures encountered.

The simpler solution is testing in a universal machine fitted with a temperature chamber. These chambers can be heated to high temperatures using resistive heaters or cooled using a liquid nitrogen flow or another equivalent gas.

NASA's thermal protection tiles are tested in a machine called Hypersonic Materials Environmental Testing System, abbreviated HYMETS. A basic diagram of the machine components is displayed in Figure 3. This machine simulates many aspects of the space and reentry environment, such as vacuum, supersonic flow and high temperature plasma impingement.

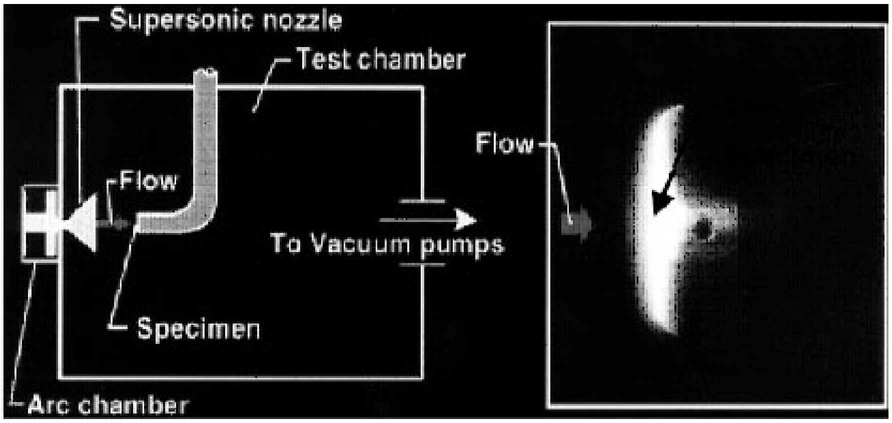

FIGURE 3 - SCHEMATIC OF NASA'S HYMET TEST CHAMBER (17)

3. THERMAL PROTECTION SYSTEMS

3.1 SHUTTLE THERMAL PROTECTION SYSTEM (NASA SHUTTLE TPS)

NASA's Space Shuttle reusable spacecraft use a very complex thermal protection system consisting of a combination of different materials, each applied in different areas of the vehicle surface to better make use of their specific capabilities. The information contained in this chapter was obtained in the NSTS Shuttle Reference Manual, available online at http://science.ksc.nasa.gov (18).

Thermal protection systems for space applications are nothing more than different materials carefully distributed. Their nature is simple and is fundamentally anchored in the underlying properties of each material, be it thermal or mechanical properties. A list of these materials and a small description of their respective properties and manufacture procedure follows.

3.1.1 Reinforced carbon-carbon (RCC)

This material is used in the leading edge of the wings and the nose cone, which are the zones subjected to the highest temperatures. RCC is a composite material, and starts as layers of graphitized rayon cloth impregnated with phenolic resin. The general aspect of a RCC panel can be seen in Figure 4. The resulting composite is pyrolized to convert the resin into carbon. The product of this operation is then impregnated with furfural alcohol and pyrolized again. The furfural alcohol also gets converted into carbon during this process.

The next manufacturing step consists in the conversion of the outer layers of the panel to silicon carbide. This is achieved by heating the panel and a dry pack (consisting of alumina, silicon and silicon carbide) to 1770ºC in an Argon atmosphere. A diffusion reaction occurs between the outer layers of the RCC and the dry pack. The silicon carbide outer layer protects the RCC from oxidation. Lastly, a layer of tetraethyl orthosilicate is introduced to minimize the susceptibility of the silicon carbide to thermal cracking.

The resulting material is an extremely light and strong material that is able to operate between -156ºC and 1649ºC (250 ºF to 3000 ºF). These materials are applied in sections subject to temperatures above 1260ºC.

FIGURE 4 - DAMAGED CARBON-CARBON PANEL (18)

3.1.2High temperature reusable surface insulation tiles (HRSI)

HRSI tiles are composed of low-density, high purity (98%) amorphous silica fibers. Ceramic bonding between the fibers forms a rigid block. The fibers only occupy 10% of the tile volume, the remaining being only air. The first step in the production of these tiles is the casting of slurry containing fibers and water to which a colloidal silica binder solution is added. After sinterization the resulting blocks are cut and machined to the required dimensions. Figure 5 shows an HRSI tile.

The tiles can have various different sizes and their thickness is dependent from the heat load they will be subjected during reentry. The maximum thickness is approximately 127 mm (5 inch) and the minimum is 25.4 mm (1 inch). The production process is finished when the tiles are coated with tetrasilicide and borosilicate glass (to provide better thermal characteristics and a silicon resin (to provide waterproofing). Image 5 shows the general appearance of a tile.

The completed tile can withstand a temperature of about 1260 ºC and sound overpressure of 165 dB. Is has a surface emittance of 0.85 and a solar absorptance of 0.85.

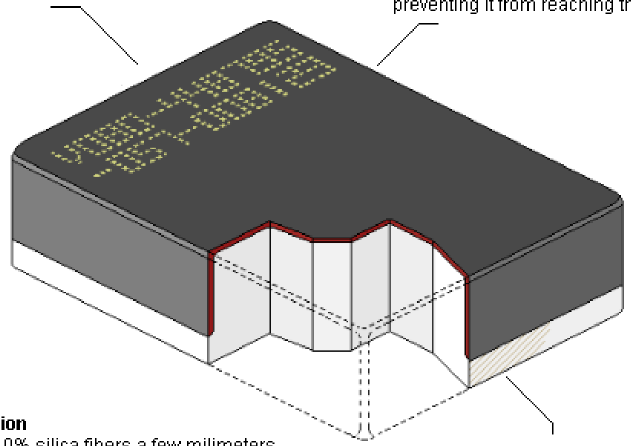

Identification number
Each tile has an identification number which tells batch and location. This number can be fed into a computer to produce an identical tile.

Coating
The outer portion of a tile is covered with a black-glazed coating of borosilicate.
These tiles do most of the coating job by shedding about 95% of the heat encountered.
The remaining 5% is absorbed by the tile's interior, preventing it from reaching the orbiter's aluminum skin.

Composition
90% air, 10% silica fibers a few milimeters thick. The tiles feels similar to plastic foam.
The silica fibers are derived from high-quality sand.

Glue
A silicon-rubber glue similar to common bathtub caulking, bonds a tile to a felt pad, that is in turn bonded to the orbiter's skin. The felt absorbs the stresses of airframe bending that could damage the tiles.

FIGURE 5-HRSI TILE

3.1.3 Fibrous refractory composite insulation tiles (FRCI)

FRCI tiles are a variation of the HRSI tiles presented above. They are stronger due to the addition of an alumina-borosilicate fiber (called AB312) to the pure silica tile slurry. The AB312 activates boron fusion and welds the micron sized fibers of pure silica into a rigid structure during sintering.

FRCI tiles have a tensile strength three times greater than that of the HRSI and can withstand a temperature approximately 37ºC (100ºF) higher. Because of their excellent thermal and mechanical properties they have replaced some of the other tiles in critical parts of the vehicle's surface.

3.1.4 Low temperature reusable surface insulation tiles (LRSI)

These tiles are also very similar to the standard HRSI already discussed. The main difference is their coating, which is white to provide passive thermal control in orbit. This coating has thermal characteristics different from the HRSI, with a surface emittance of 0.8 and a solar absorptance of 0.32.

3.1.5 Advanced flexible reusable surface insulation blankets (AFRSI)

AFRSI consists fundamentally of a low density fibrous silica batting made of high purity silica and amorphous silica fibers. This batting is sandwiched between and outer woven silica high-temperature fabric and an inner woven glass lower temperature fabric. In the next step, the three layers are sewn together to provide cohesion. Finally, the blankets are coated with colloidal ceramic silica and some more high purity ceramic fibers. This gives more surface endurance to the AFRSI. Figure 6, below, shows a complete AFRSI blanket.

FIGURE 6 - AFRSI BLANKET (18)

The finished blankets have a density of 0.12 g/cm^2 and have a thickness between 11 mm and 24 mm.

3.1.6 Felt reusable surface insulation (FRSI)

FRSI is a Nomex felt, waterproofed by a layer of silicon elastomer. This coating has a surface emittance of 0.8 and a solar absorptance of 0.32. The maximum sustained temperature of this material is 370ºC. A tile of FRSI material is displayed in Figure 7.

FIGURE 7- FRSI SHEET (18)

The following is a list of some of the properties of Nomex Felt

- Low thermal conductivity
- Non-combustible
- Dimensionally stable at elevated temperature
- High strength-to-weight ratio
- Resistant to abrasion
- Good dielectric properties
- Resistant to acids and alkalis
- Excellent flexibility

These materials require specific mounting techniques, adapted to the materials properties and the location on the structure. The following is a list of the techniques used to mount the materials presented above.

3.1.7 Reinforced carbon-carbon (RCC) panel mounting technique

RCC panels are mechanically attached to the wing leading edge by means of a series of floating joints. These joints are needed because the wing structure exhibits relatively large deflections during flight. The gap between each RCC panel is sealed with a small RCC constructed component called T-seal. These seals allow for lateral motion and accommodate the thermal expansion differences between the underlying structure and the RCC panels.

Carbon is a very good thermal conductor and the metallic inserts used to attach the panels to the wing are insulated and made in high temperature resistant alloys such as Inconel 718. This metallic inserts can be seen in the interior of the RCC panel, in Figure 8.

FIGURE 8 - CARBON-CARBON PLATE MOUNTED IN TITANIUM INSERT (18)

3.1.8 Silica tile mounting technique (HRSI, FRCI, LRSI)

Silica tiles are very rigid and cannot withstand the deformations on the airframe imposed by the forces acting on the vehicle. Stress isolation is absolutely necessary between the structure and the tiles. Strain isolation pads are used for this purpose. They are made of sheets of Nomex felt with small thickness (thicknesses available: 2.2 mm, 3 mm, and 4 mm). These stress isolation pads (SIP) are first bonded to the structure and only then the tiles are mounted.

The bonding between the felt and the structure is done with a Room Temperature Vulcanizing (RTV) silicone. The bond line is very thin (0.2 mm) to minimize weight and thermal expansion at the temperatures of 260ºC encountered during reentry and -112 ºC encountered in orbit. This bond is cured at room temperature and under pressure provided by vacuum bags.

RTV silicone is also used in a similar way to bond the ceramic tiles to the felt pads.

3.1.9 Nomex felt mounting technique (FRSI)

FRSI is bonded to the structure in the same way as the Stress Isolation Pads (SIP) are. The only difference is the thickness of the adhesive, which is considerably larger (5 mm) as the Nomex felt handles the thermal expansion more easily than the silica tiles.

3.2 METALLIC THERMAL SHIELDS

Metallic thermal protection systems are an alternative to a ceramic based system. These systems are re-radiative systems, which instead of resisting the energy influx, store it and release after. They provide high thermal insulation and are designed to maximize the re-radiation of incident heat. A metallic re-radiative thermal protection system maintains its external shape during all the portions of the flight.

Generally speaking, metallic protection shields have higher specific strength and modulus at the maximum temperature. They also have high creep strength and the used alloys provide micro-structural stability during the service life. The processing techniques are also simpler, with simplified production, sizing and handling (19).

There is a small selection of metallic alloys suitable for this application. They are listed below:

- Inconel 617
- PM 1000
- PM 2000
- Titanium aluminides (gamma and orthotrombic)
- Conventional titanium alloys

The existent solutions for metallic panels are usually sandwich structures. Lightweight thermal insulation is normally placed in the core. Some designs use a metallic honeycomb core (20).

Metallic thermal protection systems, due to their mechanical resistance, are usually connected by means of rigid mechanical connections to the structure. Fasteners and mounting brackets are responsible for the connections. These mounting accessories and other basic components of a proposed thermal heat shield can be seen in Figure 9.

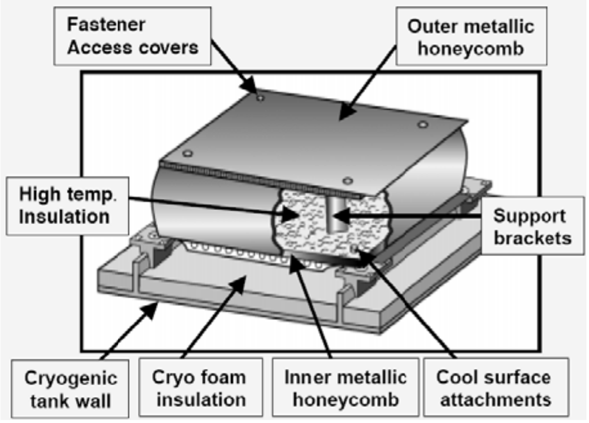

FIGURE 9 - METALLIC HEAT SHIELD (18)

3.3 ABLATIVE SHIELDING

Ablators are able to absorb large quantities of energy during the reentry by means of an endothermic chemical decomposition of the material. Phase changes also are responsible for handling and neutralizing some of the incident energy. When an ablative surface coating is subjected to the extreme temperature of reentry, the major part of the heat shield is converted into char and a small remaining thickness of ablative material performs the insulation between the structure and the hot char (20). The burnt appearance of such a shield is depicted in Figure 10.

Designing a vehicle with an ablative shield requires a careful consideration of the change of shape caused by the loss of material. The aerodynamic surface shape can be shrunk by erosion mechanisms or even increase in size due to char swelling. The nature of such changes is dependent on the main plastic constituents, the reinforcement and the aero-thermodynamic environment. As an example, reinforcement of an ablator to avoid these changes can be achieved by inserting silica fibers in a resin matrix.

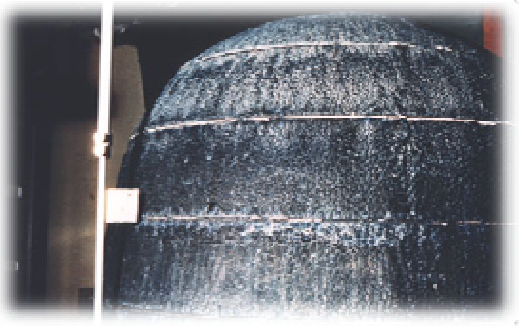

FIGURE 10 - ABLATED HEAT SHIELD (17)

Adhesive bonding is usually required to connect the ablative materials to the structure. The temperature resistance requirement of the adhesive is dependant of the thickness of ablative used and how much of the ablative material is consumed during the reentry phase.

4. EXPERIMENTAL PROGRAMME

Experimental procedures are divided in three major groups: -some procedures are intended to provide a characterization of the adhesive's mechanical properties and others are intended to analyze the combination of adhesives and the resultant mechanical behavior. Lastly another type of procedures is intended to test the joint under thermal conditions similar to an actual application.

The work focuses in the design of a high temperature joint of a heat shield. As such it is necessary to accurately define the parameters under which the joint will operate and the material to be used, so that the experimental procedures can adequately represent the problem in hand.

4.1 OPERATIONAL AND ENVIRONMENTAL REQUIREMENTS

In a normal aerospace application, the adhesive joint will be subjected to three different phases, each with its own different characteristics.

4.1.1 Launch Phase

During launch the main concern is resistance to vibration and mechanical shock. The sound pressure reaches values as high as 165 decibel (17).

- Sound pressure: 165 decibels
- Temperature change from ambient temperature to -112 ºC
- 3 G longitudinal acceleration (29,4 m/s^2)

4.1.2 Orbit Phase

During orbit the objective is to have a reasonable resistance at low temperatures. The lowest temperature is around -110ºC. Thermal differentials also appear when one part of the heat shield in sunlight and other in the shadow. This is usually passively controlled by painting the surface in different colors with different radiation absorption.

4.1.3 Reentry Phase

Reentry is the most demanding phase of all. In less than 6 minutes some parts of the surface go from -110ºC to a temperature next to 1000ºC. The aerodynamic forces acting upon the heat shield are also very substantial.

- Maximum heating rate: 1 W/m^2 (20)
- Temperature profile with the characteristics depicted in Figure 11(19)

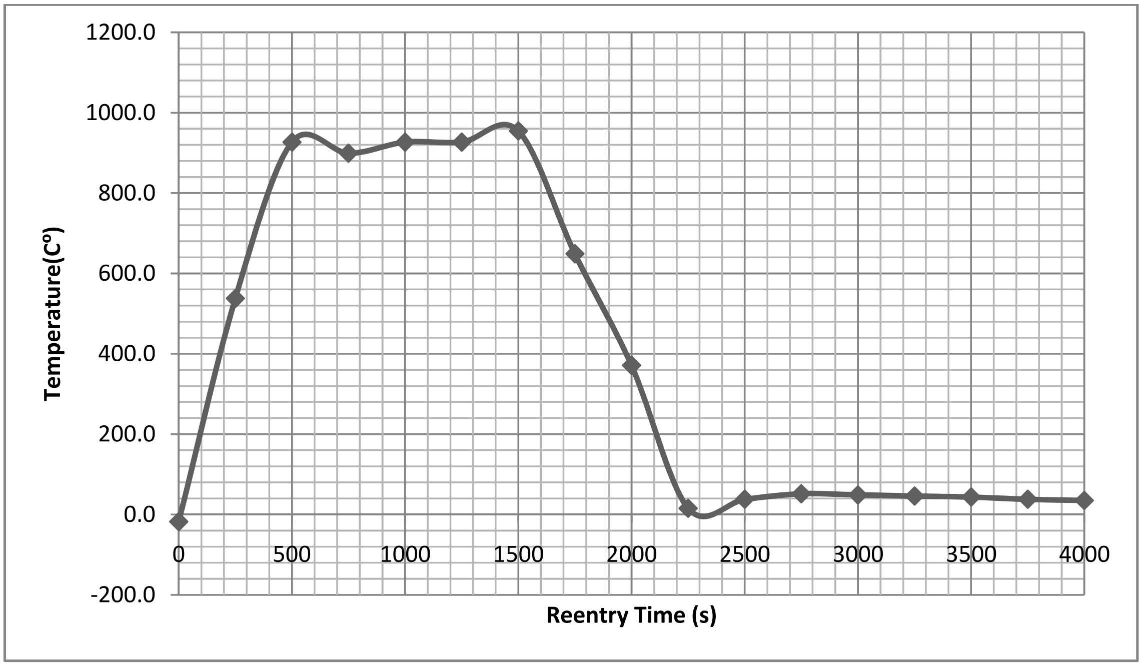

FIGURE 11- REENTRY TEMPERATURE PROFILE

- Mach number: 22 to 0

4.2 HIGH TEMPERATURE ADHESIVE SELECTION

According to the operational conditions presented above, we can identify the following requirements for the adhesive:

- High temperature resistant (1000 ºC)
- Good mechanical strength
- Single component paste preferred/easy application
- Ability to bond large areas

There are two manufacturers of high performance ceramic adhesives, Cotronics Corp (Brooklyn, New York, Unites States of America) and Aremco (Valley Cottage, New York, Unites States of America). Both companies provide a large range of products with different applications. After initial contact with these companies, each recommended one of its products for this specific application. Cotronics proposed Resbond 940SS. Aremco proposed the Ceramabond 552 silica based adhesive. A detailed property comparison is performed in Table 1.

TABLE 1- CERAMIC ADHESIVE PROPERTIES COMPARISON

	Cotronics Resbond940 SS	**Aremco Ceramabond 552**
Base	Stainless Steel	Alumina
Maximum Temperature [ºC]	n/a	1650
Maximum Continuous Temperature [ºC]	1093	n/a
Torque Strength [N/m]	n/a	9,08
Compressive Strength [MPa]	31	n/a
Flexural Strength [MPa]	17.23	n/a
Thermal Expansion [$m^3/m^3.ºC$]	$1.44x10^{-5}$	$7.74x10^{-5}$
Thermal Conductivity [W/m.K]	1.15	n/a
Dielectric Strength [Volts/mil]	Cond.	250
Volume Resistivity [ohm.cm]	Cond.	100000000
Components	2	1
Viscosity [kg/m.h]	n/a	223200
Specific gravity [g/cc^3]	n/a	2,07
Color	Grey	White
Consistency	Paste	n/a
Cure Temperature - Air Set [ºC]	22	22
Cure Time - Air Set [Hours]	4 to 8	2
Cure time @ 80ºC [Minutes]	5	n/a
Cure time @ 93ºC [Hours]	n/a	2
Cure time @ 260ºC [Hours]	n/a	2
Shelf Life [Months]	n/a	6
Storage Temperature [ºC]	n/a	9 to 30
Price (Pint, approx. 1 Kg) [USD]	50	90

According to the data shown, Ceramabond 552 appears to be the most thermally resistant adhesive (though maximum continuous temperature is not provided). It is also a single component adhesive which is preferable. However, there is relatively little information about its mechanical properties. It is also a very expensive product when compared to the alternative. Resbond 940 SS has more information regarding sustained temperature and mechanical properties. Also, the thermal conductivity is already provided which is a very important parameter to perform calculations.

Resbond 940SS, despite the fact that it is a two component adhesive, seems to be better suited for an initial study such as this. Its well detailed thermal and mechanical behavior make it better option in this direct comparison.

4.3 CERAMIC ADHESIVE CHARACTERIZATION

4.3.1 Bulk tensile testing of the ceramic adhesive

Tensile testing a ceramic adhesive is a very complex proposition, due to the high rigidity of the adhesive and the difficulty of manufacturing specimens. Two different approaches were taken to test the adhesive properties. The first approach is derived from the one used to test polymeric adhesives and consists of a tensile strength test performed on a specially shaped specimen. Although this technique is not usual, nor recommended for a ceramic material it was considered that they were worth trying, as they would provide direct comparison of properties between the ceramic adhesive and the many organic adhesives already tested before. Besides, the ceramic adhesive supposedly offers extremely high mechanical performance which can contribute to the success of this test.

The specimen design is adapted from the British Standards Institution BS 2782 standard, method 320C used to test rigid polymeric adhesives. This provides a basis of comparison between the ceramic adhesive and the polymeric alternatives.

The specimens were manufactured using a 3 part mould. A laser cut middle plate in the mould, mounted between the lower and upper bases, has the shape dictated by the BS 2782 320C standard. The adhesive was injected through a small orifice on the top base and filled the mould cavity. A vacuum pump can be used to aid in the removal of air. If the adhesive does not flow freely enough to be injected, the mould cavity can be filled directly with the top base removed. When the base is closed the excess adhesive flows escapes trough the orifices in the top base. The mould surfaces must be previously impregnated with a demoulding agent to simplify the removal process after the specimens are cured.

A drawing of the mould middle plate is presented in Figure 12 .

Once the adhesive was in the mould, it was placed in the hot plate press where it was subjected to a temperature of 80ºC. No pressure was applied as the mould itself has a set of four screws than can be tightened to provide a small but sufficient pressure. After a staging time of 5 minutes at the temperature of 80ºC the mould is cooled and the specimens are removed.

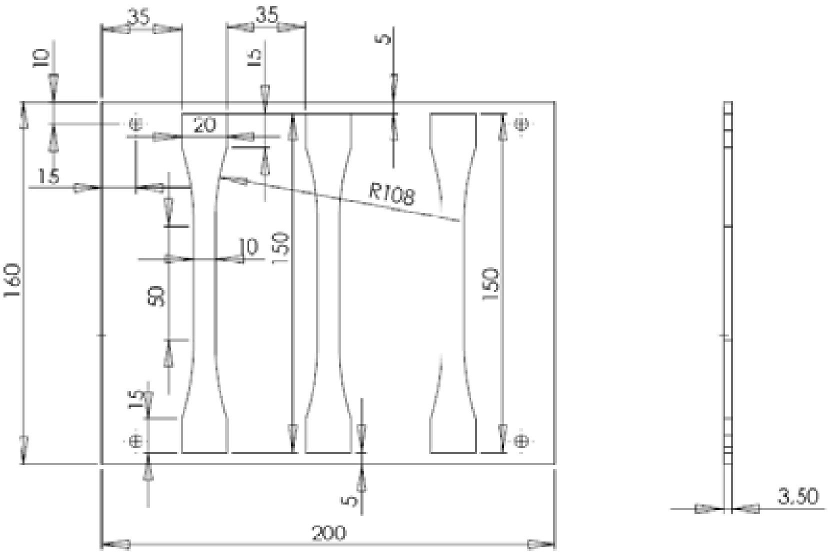

FIGURE 12- METALLIC SPECIMEN MOULD

If the metallic mould middle plate is not available, the specimens can be produced using a specially shaped silicon sheet shown in Figure 13. This method of production is simpler but the specimens have less dimensional precision. It is a variation of the technique presented by da Silva et al (21).

FIGURE 13- SILICON SPECIMEN MOULD

Tensile testing is then performed in a MTS testing machine. Strain data is obtained with an extensometer and the forces are measured with the machine load cell.

4.3.2 Flexural strength testing of the ceramic adhesive

The other approach taken to obtain basic mechanical properties for the ceramic adhesive is the three point bend test, or flexural strength test. This test subjects rectangular specimens with prescribed cross sections to a three point loading, in which the middle point is movable. This test is regulated by the ASTM C1161 standard (Standard Test Method for Flexural Strength of Advanced Ceramics at Ambient Temperature). This standard requires the specimen to have the maximum dimensions of 80x8x6 mm. These dimensions were adopted in this work.

This test can give three different parameters.

The first is the flexural stress σ_f:

$$\sigma_f = \frac{3P}{2bd^2} \tag{1}$$

The second is the flexural strain ε_f:

$$\epsilon_f = \frac{6Dd}{L^2} \tag{2}$$

The third is the Young's modulus in bending E_b:

$$E_b = \frac{L^3 m}{4bd^3} \tag{3}$$

The dimensions L, b and d are explained in Figure 14.

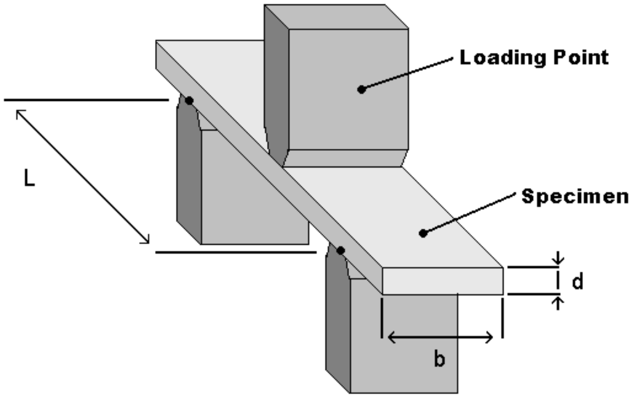

Figure 14 - Three point bend test schematic

P is the load at a given point of the deflection curve, *D* is the maximum deflection of the center of the beam and *m* is the slope of the tangent to the elastic portion of the load deflection curve.

The specimens for this test were made in a silicon mould where the appropriate shape was carved from three sheets of silicon to provide the necessary thickness. The adhesive is placed inside the mould cavity and subjected to pressure to ensure that the specimen core is free of voids. The cure can be done at 90ºC for 1 hour or alternatively at room temperature for 8 hours. The second option is safer as it reduces the thermal stresses in a large block of adhesive. The mould components and a cured specimen can be seen in Figure 15.

FIGURE 15-MOULD USED TO PRODUCE THREE POINT BEND SPECIMENS

When the curing process was completed and the specimen's mechanical properties consistent, a post-cure process is initiated. This phase consists of 1 hour at 260ºC and is meant to completely remove volatiles and remaining water from the bulk.

4.3.3 Bulk adhesive tensile test results

The production of bulk adhesive specimens was attempted for the BS 2782 320C standard, intended for organic adhesives. The construction of these specimens failed two times.

The first failure was caused by the adhesive sticking to the mould during curing. As the mould was opened, the thin specimen of adhesive broke in two halves, each bonded to the two parts of the mould.

In the second attempt the adhesive was separated from the upper part of the mould by a Teflon sheet. The sheet did in fact prevent the adhesion of the specimen to the mould but the adhesive was not cured enough to avoid the destruction of the specimen upon removal of the Teflon sheet. It was decided that this type of specimens had very low probability of being successfully produced, let alone tested, the strategy was changed and the production shifted to flexural bend specimens.

4.3.4 Flexural bending test results

The new approach consisted in the production of flexural bending specimens, according to standard ASTM C1161. Only one specimen has been completed to the time of this writing and it also has failed. For this specimen, the curing was done at 25ºC for more than 24 hours, under high pressure. This was intended to minimize the thermal stresses and assure a void free specimen. Despite the application of demoulding agent, the finished specimen could not be removed from the lower part of the mould, despite being easily separated from the upper part. Figure 16 shows the specimen stuck to the lower section of the mould. This inconsistency of the demoulding agent performed is the indication that it is not suitable for the use in ceramic adhesives. It will be replaced by a ceramic release agent before the production of the next series of specimens begins.

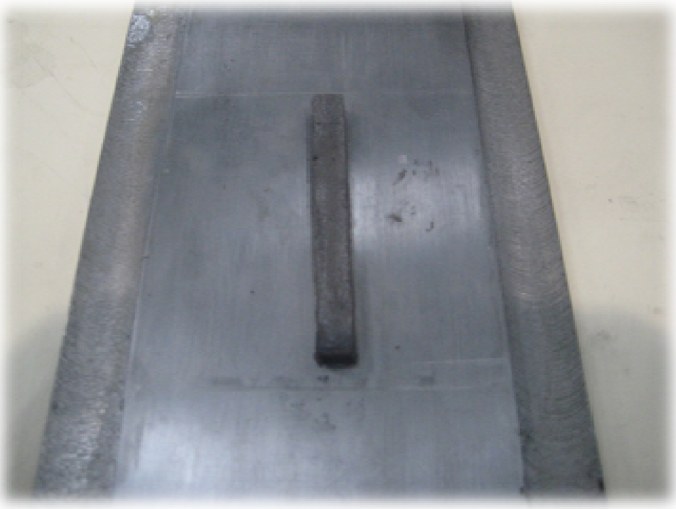

FIGURE 16-COMPLETED FLEXURAL BEND TEST SPECIMEN

4.3.5 Single lap joint testing of ceramic adhesive

Single lap joint testing is probably the best experimental procedure to quickly assess the bond performance. It consists in two simple rectangular plates which are bonded in an overlapped area.

The substrates used for this test are metallic, made of high stiffness steel. They are sand blasted with alumina before bonding to prepare the surface for optimal adhesion properties.

The specimens were produced in a special mould, which holds the substrate plates at the appropriate distances. Spacers are placed to keep the upper specimens at a specified distance. This distance is the adhesive layer thickness. The mould is depicted in Figure 17.

FIGURE 17 -MOULD USED TO PRODUCE SINGLE LAP JOINT SPECIMENS

The specimen dimensions are introduced in Figure 18.

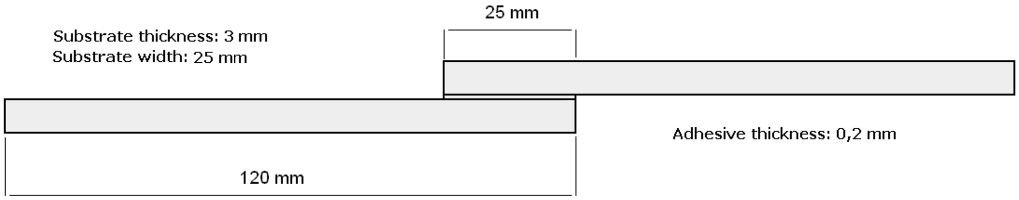

FIGURE 18-SINGLE LAP JOINT SPECIMEN DIMENSIONS

The mould containing the specimens was placed in a hot plate press. The curing procedure consisted in the application of pressure and of temperature for approximately 1 hour. The temperature used was 90ºC. The pressure is needed to expel the excess adhesive from the joint and therefore reaching the correct adhesive thickness. After this curing stage the specimens are slowly cooled and brought back to ambient temperature.

4.3.6 Single lap joint test results

Similarly to the bulk specimens, single lap joint specimens also suffered from severe manufacturing problems. The completed specimens were not actually tested as they all failed when being bolted to the testing machine, demonstrating their extreme fragility. This was caused by slight bending in the steel substrates. It is thought that this slight deformation in the substrates was caused by the post cure process at 270ºC.

The fracture surfaces of these specimens were inspected and photographed (Figure 19 and Figure 20) and it was found that they had extremely low quality, filled with voids and imperfections. The resistance to flow of the ceramic adhesive requires extremely high pressures to achieve the correct layer thicknesses and elimination of defects. In this case, the low pressures used (500 kgf) were not sufficient to homogenously distribute the adhesive on the joint. Despite this the failure was cohesive in the adhesive, which leads one to conclude that the surface preparation is correct and not cause of this low resistance.

FIGURE 19-FRACTURE SURFACE OF SINGLE LAP JOINT SPECIMENS (1/2)

FIGURE 20-FRACTURE SURFACE OF SINGLE LAP JOINT SPECIMENS (2/2)

4.3.7 Thick Adherend Shear Testing

The TAST (Thick Adherend Shear Test) is an experimental procedure used to obtain the shear properties of an adhesive. This test is done with thick metallic substrates connected by a joint designed work almost exclusively in a shear stress loading. The dimensions of the adherends are dictated by the applicable ISO norm, ISO 11003-2.2 and are displayed in Figure 21.

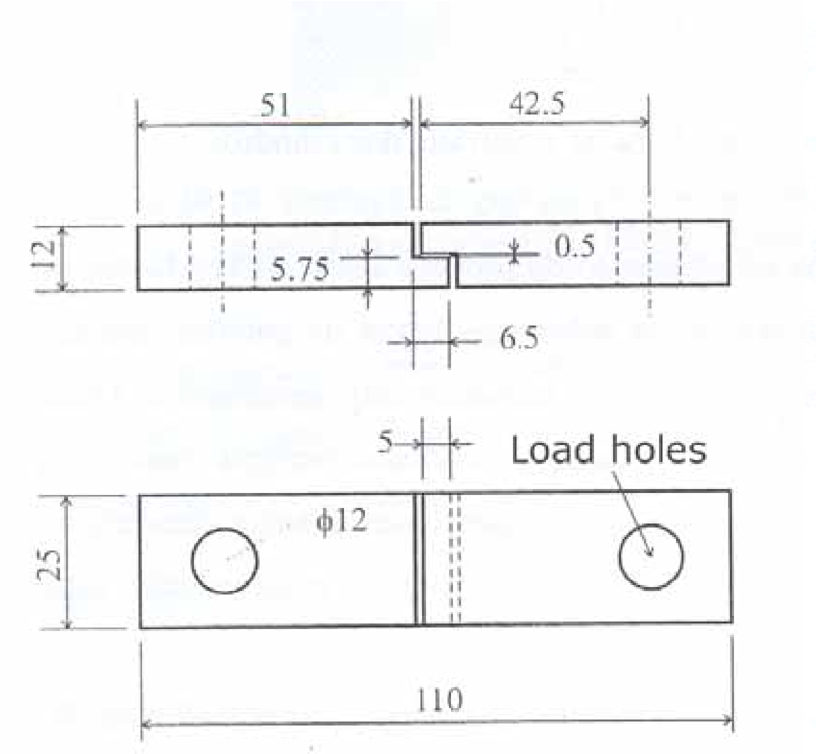

FIGURE 21-TAST SPECIMEN (DIMENSIONS IN MM)

The standard for this test recommends using two transducers for deformation measurement. These are mounted in each side of the adherend, to compensate for eventual flexion deformations. As the transducers are mounted in the metallic substrate, the indicated deformation is a combination of the between the adhesive and adherend deformation. To account for this fact, the ISO 11003-2 norm requires a correction to be made, using data from a dummy specimen, built only with the adherend material. In the present work, the adherend displacement was measured by a convention strain gauge (with a 25 mm reference length). The correction for the steel deformations was performed via a calibration procedure.

Specimens for TAST were produced in a specially designed mould. This mould is sized to suit the short and thick substrates used in this test. Figure 22 depicts this mould and some specimens being manufactured. The detailed production procedure of these specimens is listed below:

- Mould cleaning: The mould was cleaned with acetone to remove contaminants such as grease and oils.

- Mould heating: The mould was placed in the press and heated to 70ºC in preparation for the mould release application.

- Mould release agent application: Mould release agent is applied to all the mould surfaces and to the small metallic spacers. The agent was applied in three consecutive passes to ensure perfect coating.

- Adhesive application: The lower substrates were placed in the mould and adhesive was placed in the middle section (the section parallel to the traction force direction). Two metal spacers were placed in each specimen to separate the surfaces perpendicular to the traction force direction. This is what ensures that the joint is subjected to shear stresses only.

- Curing: The mould was closed and placed in the press. A curing temperature of 100ºC is used with a curing time of just 10 minutes. After the cure process is completed the mould is slowly cooled and the specimens are removed.

FIGURE 22 --TAST SPECIMENS IN MOULD

The specimens were then tested to failure in a MTS testing machine. Strain information was obtained using an extensometer but can also be derived from a video of the test, using digital post processing techniques.

4.3.8 TAST results

TAST specimens were also unable to be produced satisfactorily with the ceramic adhesive. Of the four specimens produced only two survived the removal from the mould. These two specimens were then tested in a universal testing machine to try to obtain the shear stress curves. Unfortunately the specimens failed at very low loads without generating any kind of strain-stress curve. The extremely low forces at failure are listed in Table 2.

TABLE 2-TAST FAILURE LOADS

Specimen	Failure load (N)
1	27
2	142

The fracture surfaces for this test (Figure 23), contrast with the single lap joint fracture surfaces, as they have much better quality, absent of voids and other imperfections. The failure was also cohesive in the adhesive, reinforcing the idea that the surface preparation is adequate. Considering the appearance of the fracture surface, the low values of joint strength can only be explained by three different possibilities:

- Incomplete/Incorrect curing procedure: Although the adhesive manufacturer’s recommended curing procedure and mixture ratio was followed, it is possible that for some joint geometries, significantly longer curing times are required.

- Thermal/Pressure cracking: The fragile nature of the adhesive makes it very susceptible to residual stresses. The manufacturing process of these joints might have to be completely redesigned to be able to deal with these special adhesives.

- Inadequate adhesive: The adhesive itself might not be the best for this application. The selection process was performed with the help of the adhesive manufacturer but it is always possible that this specific product is not able to be employed in adhesive joints.

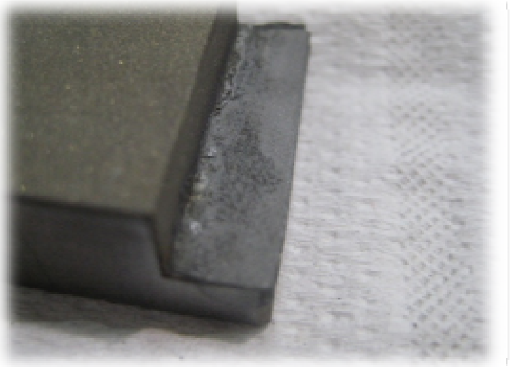

FIGURE 23- TAST SPECIMEN FRACTURE SURFACE

4.4 DUAL ADHESIVE COMBINATION

The use of two adhesives is one of the techniques that might provide a good solution for applications with large temperature gradients. Because we are dealing with vastly different demands in the ends of the spectrum we also require a wide range of properties from the adhesive joint. In this case, the use of two different adhesives can provide us with the necessary wide range of properties.

As this work focuses in extremely high temperature adhesives, the first possible adhesive combination that comes to mind is the combination of a ceramic adhesive with high temperature silicon. If the combined properties of this pair of adhesives can be harnessed one would obtain a strong joint both at high temperature (where the ceramic adhesive would be needed) and low temperature (where the ductile RTV silicone would be able to carry the load). The main problem posed by this approach is fundamentally the ability of one adhesive to survive in the conditions that are most unfavorable for it. The definition of the temperature limits for each of the adhesives is not easy, as although we have information relative to the operational limits (those limits at which the adhesive will sustain a significant load) we do not possess information regarding to the temperature they can achieve without incurring in permanent damage. The best way to obtain this information is to perform high temperature testing of the adhesives.

As the ceramic adhesive testing is still in a very preliminary phase and the RTV silicone is still being sourced, some simple tests were devised using adhesives that already existed in our laboratories stock. Adhesives with very different rigidity modulus were selected, as this simulates the Ceramic-RTV configuration.

For the role of high temperature adhesive (HTA) Araldite AV 137 epoxy based adhesive was chosen. This is a two part adhesive that requires a hardener (HV996). Table 3 lists the basic adhesive mechanical properties (14).

TABLE 3-ARALDITE AV138 MECHANICAL PROPERTIES

Property	Value
Young Modulus	4590 MPa
Tensile Strenght	41.01 MPa
Elongation at break	1.3%

For the role of low temperature adhesive (LTA) we chose Araldite 2015. This is a very versatile adhesive reasonable strength and an average modulus of elasticity. This adhesive has already been tested for the author's "Projecto de fim de curso" work and some of the properties obtained are listed in Table 4.

TABLE 4-ARALDITE 2015 MECHANICAL PROPERTIES

Property	Value
Young Modulus	1850 MPa
Tensile Strength	22.5 MPa
Elongation at break	4.4%

4.4.1 Araldite 2015 and Araldite AV 138 combination

These two adhesives work as the baseline for the study in the combination of different adhesives. These two adhesives have a significant difference in Young's modulus and can in a way represent the behavior that a ceramic adhesive will have when combined with a much less rigid adhesive. This combination is used to identify some of the major parameters that have influence in dual adhesive connections. Among these parameters is the existence of an angled taper in the end of the joint.

The angled taper was intended to minimize the stresses in the tip of the joint and is a valid solution when considering very rigid adhesives. The use of angled tapers can provide interesting mechanical properties for this case. Reduced peel stresses at the tip and better fatigue behavior are mentioned in various examples in the literature (22) (23).

For comparison purposes, tests were performed in specimens with both adhesives and with each adhesive separately. Different taper geometries are also analyzed. For each taper of each adhesive three different specimens were produced. The combinations manufactured are listed in Figure 24, Figure 25, Figure 26 and Figure 27.

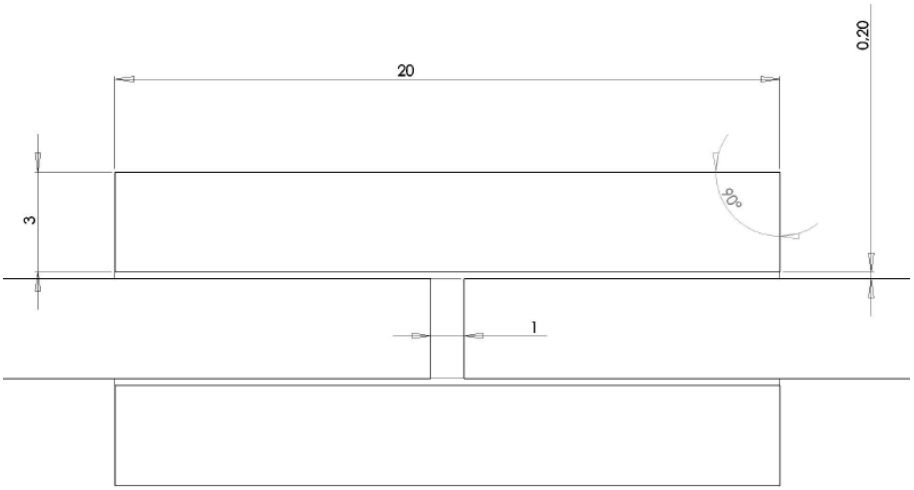

FIGURE 24 - 90° TAPER (NO TAPER) – ARALDITE 2015; ARALDITE AV138; ARALDITE 2015 + AV138 (DIMENSIONS IN MM)

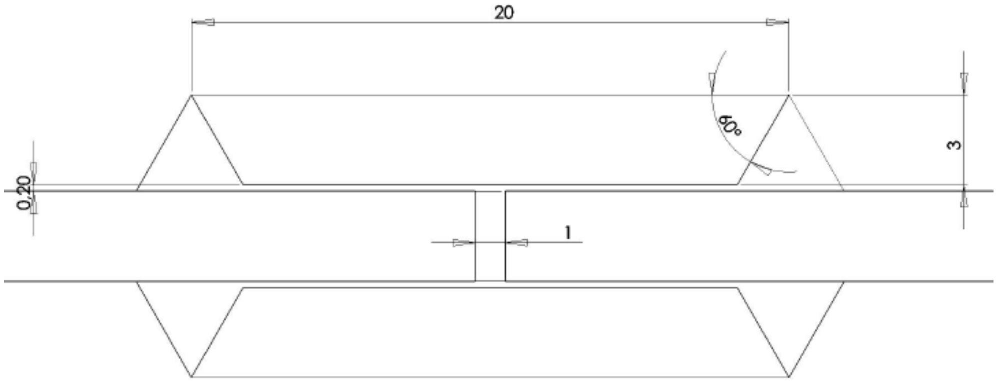

FIGURE 25- 60° TAPER – ARALDITE 2015; ARALDITE AV138; ARALDITE 2015 + AV138 (DIMENSIONS IN MM)

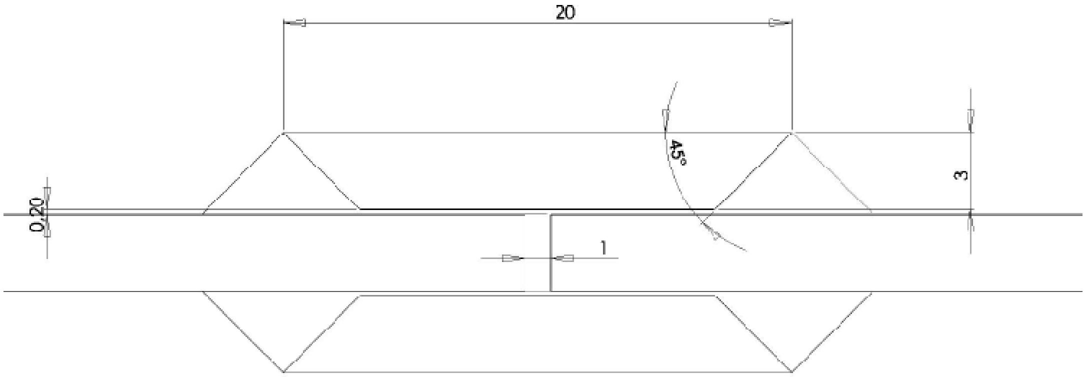

FIGURE 26- 45° TAPER – ARALDITE 2015; ARALDITE AV138; ARALDITE 2015 + AV138 (DIMENSIONS IN MM)

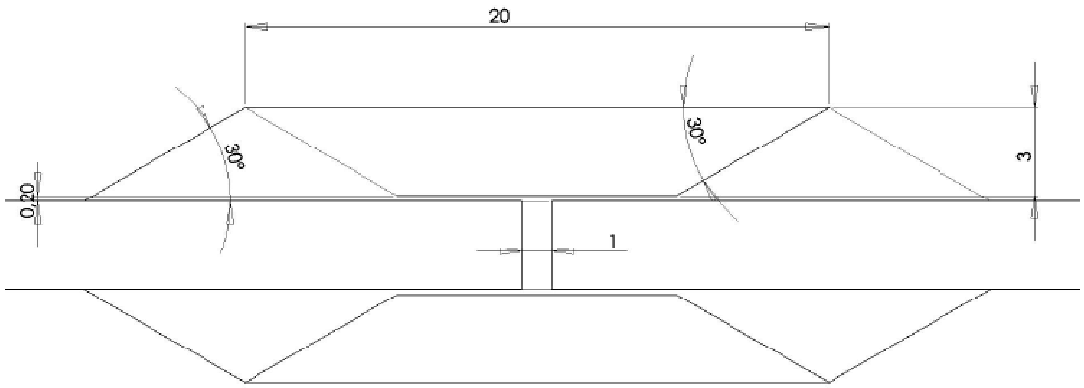

Figure 27- 30° Taper – Araldite 2015; Araldite AV138; Araldite 2015 + AV138 (dimensions in mm)

When a combination of two adhesives was used there was the need to select the length that each adhesive would occupy in the adhesive layer. The main concern here was for this length to be the same in all of the different configurations studied. The 30º taper angle is the main limitation in this case as it restricts the area available to place a separation barrier. Figure 28 shows the location of this barrier.

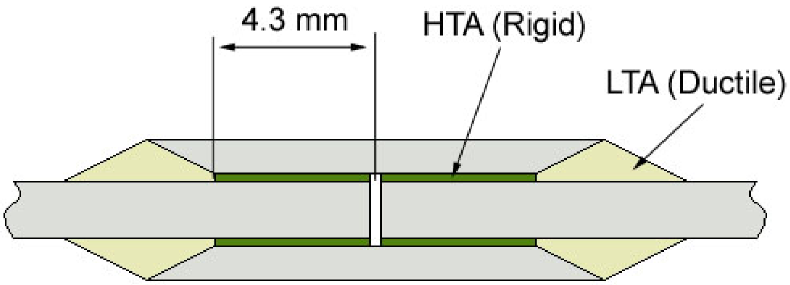

Figure 28- Location of seperation barrier and placement of adhesives (valid for all taper angle values)

The total overlap lengths with the current geometry are listed in Table 5.

Table 5-Overlap lengths for each adhesive

Adhesive	Length
HTA (center of the joint)	9.6 mm
LTA (tapered zones)	10.4 mm

This procedure also provides some experience with the manufacturing of dual-adhesive joints, as these require special technique to be performed in a satisfactory fashion. Different methods of separation were tested. It was found that the most effective method was the use of a nylon line with the same thickness of the adhesive layer between the adhesives. The nylon line is glued using a small amount of cyanoacrylate to the substrates. This method gives a very good dimensional control and occupies a very small area when compared with other techniques tested (use of small strips of silicone or Teflon). The appearance of a separation barrier can be seen in Figure 29.

The process of construction requires the same mould as the one required to produce single lap joint specimens. The mould geometry aligns the substrates, patches and moulds. The construction must follow a special sequence due to the number of different components that make up each specimen. The sequence is illustrated in Figure 30.

FIGURE 29- BARRIER USED IN DUAL ADHESIVE JOINT CONSTRUCTION

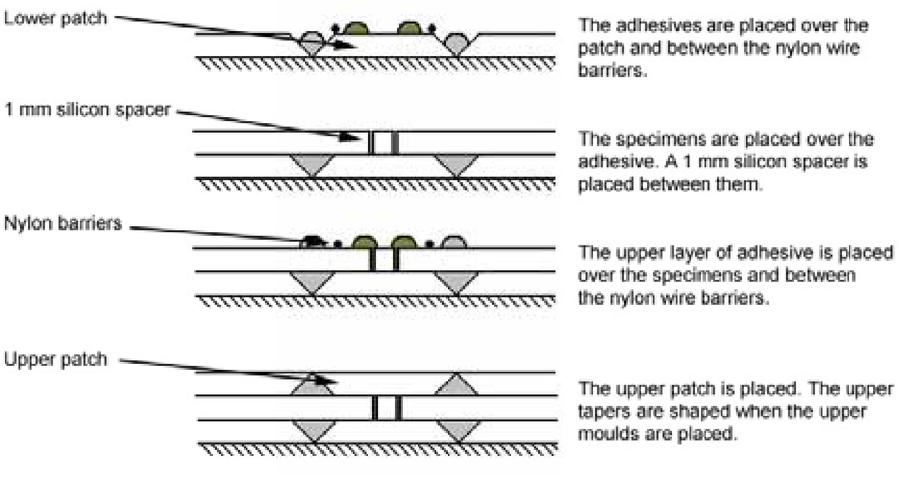

The adhesives are placed over the patch and between the nylon wire barriers.

The specimens are placed over the adhesive. A 1 mm silicon spacer is placed between them.

The upper layer of adhesive is placed over the specimens and between the nylon wire barriers.

The upper patch is placed. The upper tapers are shaped when the upper moulds are placed.

FIGURE 30- DUAL ADHESIVE JOINT CONSTRUCTION PROCESS

Once the specimen production was complete, the mould was closed and placed in a hot plate press. The force imposed on the mould was around 800 kg, enough to press each component into position and ensures the correct adhesive layer thickness. The curing temperature was chosen according to the slowest curing adhesive. In the specific case of the combination of Araldite 2015 and Araldite AV138 the curing times are very similar and a time of one hour at 60ºC is used. This temperature was relatively low and it is chosen to minimize the appearance of thermal stresses.

The completed specimens were then subjected to a tensile test in an Instron testing machine. The joint displacement was measured with a 50 mm extensometer. Three specimens were produced of each taper angle for each adhesive combination. The list of specimens produced is presented in Table 6.

TABLE 6- LIST OF SPECIMENS PRODUCED

Taper Angle	Material combination and number of specimens
90 degrees	3 specimens with Araldite 2015 3 specimens with Araldite 2015 in the taper and Araldite AV138 in center 3 specimens with Araldite AV138
60 degrees	3 specimens with Araldite 2015 3 specimens with Araldite 2015 in the taper and Araldite AV138 in center 3 specimens with Araldite AV138
45 degrees	3 specimens with Araldite 2015 3 specimens with Araldite 2015 in the taper and Araldite AV138 in center 3 specimens with Araldite AV138
30 degrees	3 specimens with Araldite 2015 3 specimens with Araldite 2015 in the taper and Araldite AV138 in center 3 specimens with Araldite AV138

To gain a better insight into the parameters that influence joint behavior and learn new techniques, a couple of different materials and joint combinations were also tested.

The first of these tests was the production of joints using carbon patches. This was done mainly to study the behavior of Araldite 2015 when bonding composites to metals. The specimens produced had a very simple geometry, with a 25x20x1 mm carbon fiber-phenolic resin patch bridging a 1mm gap. The carbon patches had the fibers placed uni-directionally and these were lined with the direction of the load. Aluminum substrates were subjected to sandblasting and degreasing. This provides a good surface for the epoxy adhesive. The carbon patches were lightly abraded with sandpaper. The joints were assembled in the mould used for the single lap joint specimens presented above and subjected to a cure at the temperature of 70ºC for approximately 1 hour. After curing, the specimens were tested in an Instron tensile testing machine.

A second set of experimental procedures was performed with the same geometry and configuration of the Araldite 2015+ Av138 tests.

In this case the Araldite 2015 adhesive was moved to the center section of the joint and acrylic adhesive, acting as the HTA and, 3M DP-8005, was applied in the external zone of the joint, in the tapered sections. This adhesive has a low Young's modulus, and was used to better understand the influence of the adhesive stiffness in the strength of a tapered joint. The basic mechanical properties of this adhesive are listed in Table 7.

TABLE 7- 3M DP-8005 MECHANICAL PROPERTIES

3M DP-8005 mechanical properties	Value
Young Modulus	590 MPa
Stress at peak load	13 MPa
Strain at peak load	5.3%

Specimens were produced in the 90º (no taper) and 60º configurations. For each of these configurations three different specimens were assembled. The specimens were subjected to a 70ºC cure for 1 hour in a hot plate press. After curing they were tested in a universal testing machine. The joint displacements were measured with a 50 mm extensometer and the forces with the machine load cell.

4.4.2 Tapered specimen testing results

The results of tensile testing of the single and dual adhesive specimens are listed in Table 8. The complete load-displacement curves for the tests can be consulted in Annex A.

TABLE 8- TENSILE TEST DATA 1

	Maximum tensile strenght (kN)		
	2015	**2015+AV138**	**AV138**
90 Average	10.69	11.15	9.95
90 Standard deviation	0.53	1.16	0.85
60 Average	11.01	11.37	12.26
60 Standard deviation	0.03	0.56	0.44
45 Average	10.46	11.84	13.30
45 Standard deviation	0.51	0.73	0.48
30 Average	10.30	10.48	11.97
30 Standard deviation	0.51	0.39	0.77

This table demonstrates that the joint strength of rigid adhesives can be significantly increased by use of a taper angle. This effect is not as visible when less rigid adhesives are used alone or in the taper. The gains of performance verified for AV138 are summarized in Table 9.

TABLE 9 - RELATIVE JOINT STRENGHT IMPROVEMENT

Taper angle (degrees)	Joint Strength (percent)
90	100
60	123
45	133
30	120

Another interesting fact is the synergetic combination of adhesives in the taperless configuration. Here we see that the combination of adhesives is stronger that any of the adhesives individually. This is explained by the sensibility to stress risers of the AV138 adhesive. This is a very stiff and strong adhesive, but performs badly in unfavorable conditions, such as the abrupt patch termination zone. When 2015 is placed in that area it resists better than AV138 would resist itself and the result is a joint better than any of the adhesives alone could provide. Preliminary results were also obtained for the combination between Araldite 2015 and 3M DP8005 and the repair with the carbon patch. These results are presented in Table 10.

TABLE 10-TENSILE TEST DATA 2

	Maximum tensile strenght (kN)	
	2015+ DP8005	**Carbon Patch +2015 Adhesive**
90 Average	3.38	6.38
90 Standard deviation	0.31	0.31
60 Average	3.29	n/a
60 Standard deviation	0.21	n/a

The results obtained with 3M's DP8005 adhesive corroborate the notion that the use of tapers is ineffective with low stiffness adhesives, as we see a reduction of strength for the testes 60º taper angle.

The results regarding the carbon fiber composite patch cannot be compared directly with any other tested case and serve only as a rough indication of the level of strength that can be obtained by bonding composite and aluminum.

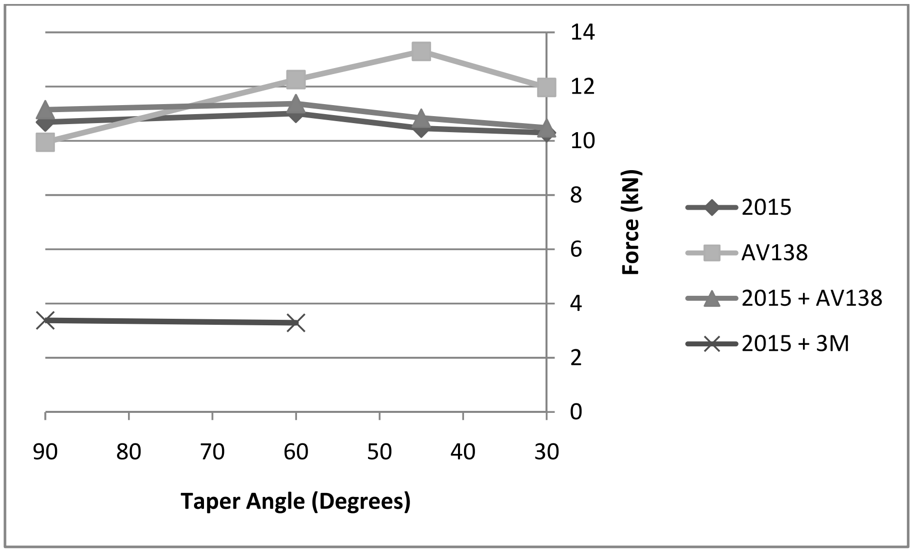

FIGURE 31- JOINT STRENGTH EVOLUTION WITH TAPER ANGLE

Figure 31 summarizes the evolution of maximum force verified for each angle. We see that the stiffest adhesive has a peak around 45º, falling off immediately after. 2015 and 2015+AV138 have almost identical distributions, owing to the fact that it is the adhesive in the taper of the joint that dictates the effectiveness of the taper. In these two cases it is the same adhesive, so similar distributions are expected. The less rigid 3M adhesive, as explained before, does not benefit from the taper angle and this is easily visible here.

It is important to register and analyze the surface fractures of each specimen so that defects and imperfections can be identified. These imperfections must be reduced to a minimum so that the results are as consistent as possible. It is also necessary to identify if the failure is adhesive or cohesive, so that the surface preparation methods can be evaluated and their effectiveness asserted. Some pictures of the fracture surfaces are listed below and commented.

FIGURE 32- 2015+ AV138 90 DEGREES TAPER FRACTURE SURFACE

Infiltration of adhesive into the other side of the separation barrier is common during specimen preparation. The amount of adhesive is usually small as Figure 32 demonstrates and therefore the influence in the final result is negligible. We can identify totally cohesive failure of both adhesives and we can also notice that the taper base is one of the points of failure. This is an atypical case as most of the failures occurred in the interface between the patch and the adhesive taper.

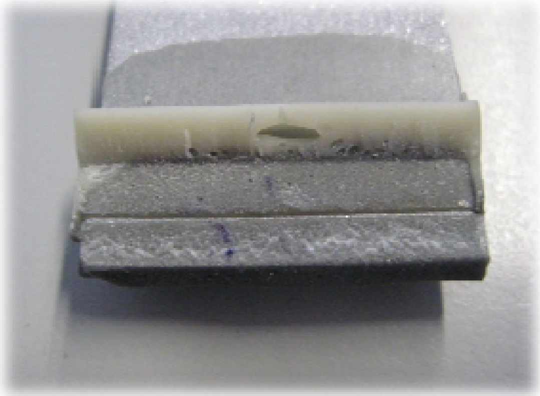

FIGURE 33- 2015+AV138 60 DEGREES TAPER FRACTURE SURFACE

In Figure 33 we can identify a large void in the taper. This void results from the taper's manufacturing process where large amounts of adhesive are applied over the specimen. Air can get trapped under the successive strings of adhesive and expands during cure resulting in these voids.

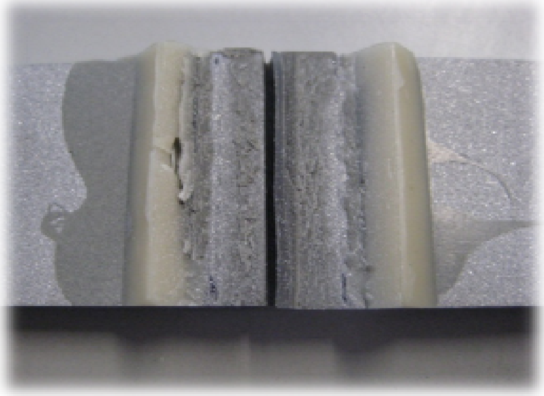

FIGURE 34- 2015+AV138 45 DEGREES TAPER FRACTURE SURFACE

Figure 34 is very similar to the previous. It demonstrates the typical location of the failure, between the taper and the patch (missing). In this case the failure appears to have initiated in a void.

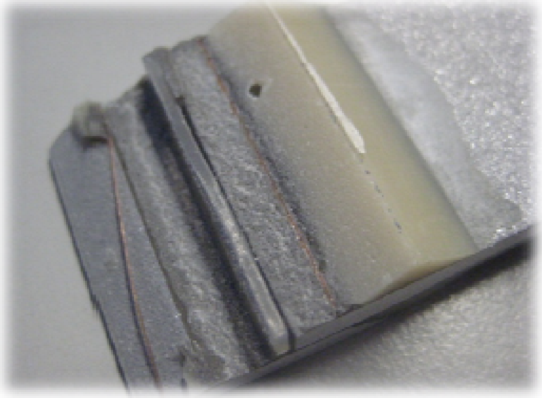

FIGURE 35 - 2015+AV138 30 DEGREES TAPER FRACTURE SURFACE

In Figure 35 another small imperfection in the taper can be seen, coupled with the usual failure surface between the taper and the adhesive taper.

Figure 36- AV138 90 degrees taper fracture surface

In Figure 36 we observe the characteristic cohesive failure surface of AV138 adhesive. The patch was ejected during testing.

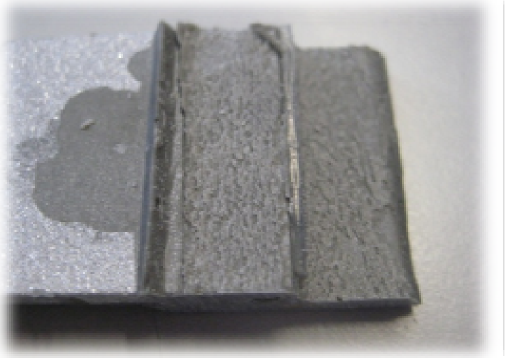

Figure 37 - AV138 60 degrees taper fracture surface

This example, Figure 37 shows the rough surface of the taper, which contrasts with the usually smoother surface of the taper in the Araldite 2015 fracture images. Here the failure clearly propagates more irregularly, consistent with the behavior of a rigid adhesive.

FIGURE 38- AV138 45 DEGREES TAPER FRACTURE SURFACE

Figure 38 clearly shows that this adhesive is very stiff. Pieces of the taper have broken off completely. The cracks propagate in different directions, especially near the tip where the stress risers are more important. Small voids are also visible in the adhesive

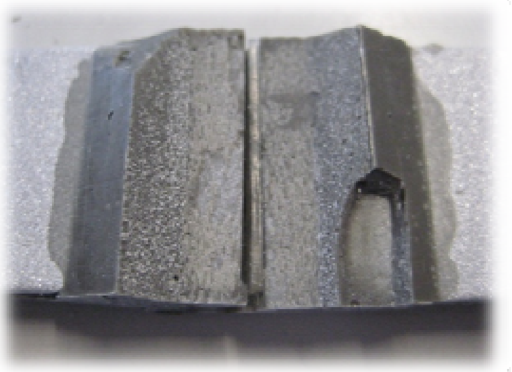

FIGURE 39- AV138 30 DEGREES TAPER FRACTURE SURFACE

Figure 39 is almost a carbon copy of the case presented above, only with a different taper angle. It serves to demonstrate that the ejection of large amount of the taper section is a typical phenomenon with these stiff adhesives and resultant from high local stresses.

5. SIMULATION PROGRAMME

5.1 THERMAL SIMULATION

A thermal simulation using EES software (Engineering Equation Solver) is useful to determine an ideal configuration to withstand the energy flux during reentry. We can easily study the effect on the heat shield performance of material properties, thicknesses and location.

For this analysis a very simple thermal barrier was considered. This barrier consists of three components. First we have a low density, high thermal resistant silica tile. This tile acts as the main thermal barrier to the heat input. It is also the thickest component of the system and this thickness is designated Ls. Next we have a ceramic adhesive layer. This adhesive is responsible for keeping the tile affixed to the main structure of the hypothetical vehicle or machine using this heat shield. The adhesive layer must obviously be thin when compared with the silica tile. This thickness is referred as La. Finally we have a metallic layer, intended to represent the outer layer of the vehicle structure. The thickness value is represented as Lm.

The system has incident power as thermal input and the final metallic layer transmits heat trough convection to the interior of the structure. If we consider a large heat shield with uniform heating we can assume that there will be no transfer of energy trough the sides of the heat shield.

This is a very simplified model, especially if we consider the detailed nature of the actual thermal protection systems, presented in a previous section of this work. A real thermal system will have layers of material introduced to accommodate torsions in the structure without damaging the ceramic heat shield.

A sectional view of the thermal system can be represented by the diagram in Figure 40.

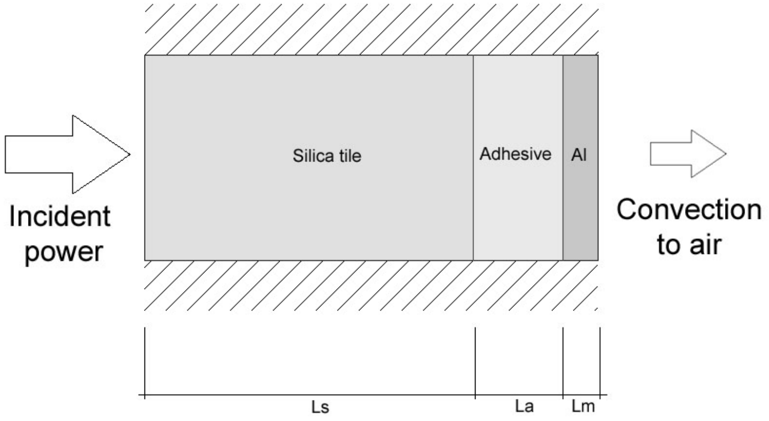

FIGURE 40-THERMAL MODEL

A heat influx acts directly over the silica tile of the heat shield. This heat influx can be adjusted to provide a temperature of approximately 1000ºC. This value is selected according to the graph presented in the chapter that lists the operational conditions.

To study this thermal problem we must also create a diagram of equivalent resistances, shown in Figure 41. This is also a simplified representation that takes into the account the method of heat transfer in each section of the heat shield.

FIGURE 41-THERMAL RESISTENCES DIAGRAM

If we analyze this diagram from left to right, we first see the heat input to the system. This heat is obtained from the surface area of the heat shield and the incident power applied. The next component is the equivalent heat resistance imposed by the silica heat shield. This resistance is expressed by the K parameter in W/m.K. This parameter is typical of each of the materials. In this case, the type of heat transference is designated conduction.

If we look further to the right in the diagram we find the equivalent resistances for the adhesive and the aluminum base. These resistances operate exactly as explained for the silica tile. The mode of heat transfer is still conduction.

The last component of the diagram is the thermal resistance for the convection in the air behind the heat shield. This is represented by the variable h, specific for each gas or mixture of gases. The units for h are $W/m^2/K$.

The calculation of temperatures in this transient model is performed using a finite difference formulation called the implicit formulation. This formulation has the following appearance:

$$\tau T_{m-1}^{i+1} - (1+2\tau)\tau_m^{i+1} + \tau T_{m+1}^{i+1} + \tau \frac{g_m^{i+1}\Delta x^2}{k} + T_m^i = 0 \tag{4}$$

It is an iterative calculation method that calculates the temperature for each node in the next step T^{i+1} using information from the nodes that surround it, T_{m-1} and T_{m-1}. The *x* parameter is the distance between nodes in the calculation step and is expressed in meters.

The τ variable represents a dimensionless parameter called the mesh Fourier Number. This is the ratio of the heat conduction rate to the rate of thermal energy storage.

$$\tau = \frac{\alpha \Delta t}{\Delta x^2} \tag{5}$$

The α variable represents the thermal diffusivity of the wall material. It is expressed by the next equation:

$$\alpha = \frac{k}{\rho C} \tag{6}$$

The parameter k is the thermal conductivity of the wall material, presented in W/m.K. The density of the wall material is represented by ρ and expressed in kg/m^3. Finally C represents the specific heat of the material. It is the measure of the heat energy required to increase the temperature of a determined quantity of substance for a certain temperature interval. It is expressed in J/kg.K.

Table 11 shows the values of these properties used for each material in the thermal model.

TABLE 11-THERMAL PROPERTIES OF THE HEAT SHIELD MATERIALS

Material	K(W/mK)	P(kg/m^3)	C(J/kgK)
Silica Tile	4	144	0.84
Ceramic Adhesive (940SS)	1.44	2000	10
Aluminium Alloy	177	2700	896

The model finite differences model is implemented using the EES software (Engineering Equation Solver). Seven nodes are used to perform calculations. The nodes are listed in Table 12.

TABLE 12- NODE LOCATIONS

Node number	Location
0	Outer wall (silica)
1	Wall core (silica)
2	Interface (silica-adhesive)
3	Wall core (adhesive)
4	Interface (adhesive-Al)
5	Wall core (al)
6	Inner wall (al)

The model allows control of the wall thicknesses and the input power. The simulation procedure runs the evolution of the transient model in 10 intervals of 60 seconds each representing a total time of 10 minutes. This allows the visualization of the temperature gradients along the heat shield. The complete thermal model's code is presented in Annex B.

The thermal simulation is performed using two values as reference points. The first of these reference points is a surface temperature in the silica tiles of around 1000ºC. In page 34 of this work we can see Figure 11 which shows that the maximum temperatures in the silica tiles are around 1000ºC. The second point is the length in time of the heating stage. Consulting that graph and other references we find that the heating phase lasts between ten an fifteen minutes. Using this data, the models constructed have a temperature at the outer surface as close as possible to 1000ºC and run for 10 minutes.

Three different models were run in EES. The models differ essentially in the wall thicknesses and the amount of thermal energy that flows through them. The first model, called A, wall thicknesses are represented in Table 13- "A" Model Wall Thicknesses.

TABLE 13- "A" MODEL WALL THICKNESSES

Component	Model 1 length (mm)
Silica (Ls)	120
Adhesive (La)	10
Aluminum (Lm)	6

The extremely thick adhesive layer (10 mm) of model A is obviously unrealistic and only intended to provide more information about the heat blocking capacity of the adhesive. This model needed a heat influx of 21 kW/m^2 to achieve a surface temperature of 1005º. The temperature distribution after 10 minutes of heat is given in Figure 42. The temperature in the aluminum inner wall is 228 ºC

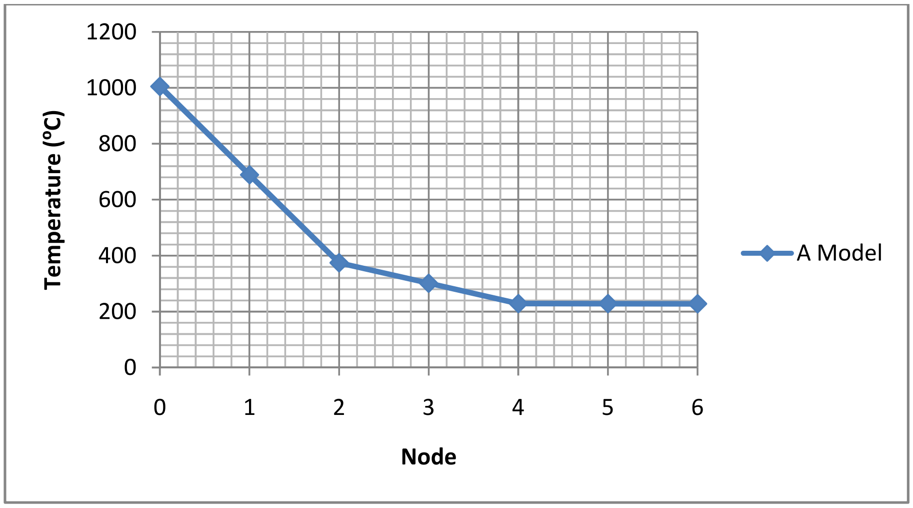

FIGURE 42-TEMPERATURE DISTRIBUTION ALONG THE "A" MODEL

The temperature in the core of the adhesive is given by Figure 43.

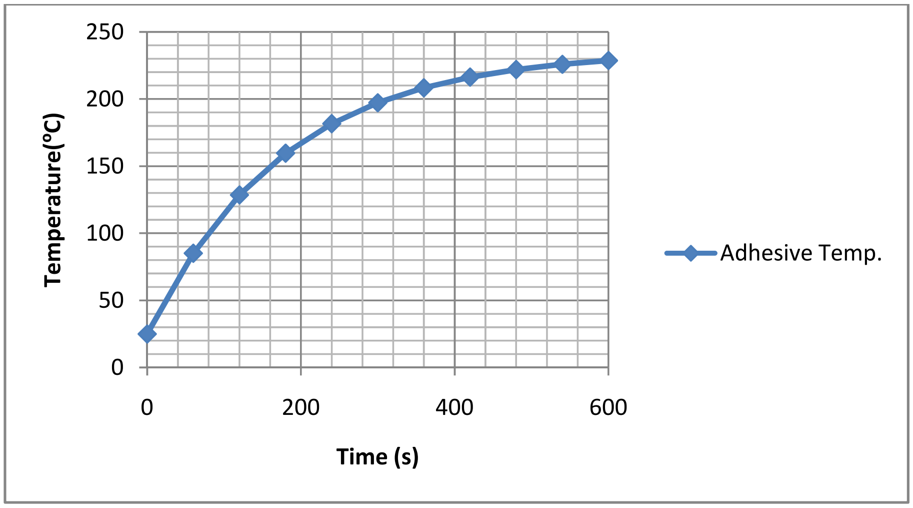

FIGURE 43-ADHESIVE CORE TEMPERATURE VARIATION WITH TIME

The maximum temperature verified in the core is 228.7 ºC.

The second thermal model is called "B" model. This model keeps the adhesive and aluminum walls with the same thickness but reduce the silica tile in half. Table 14 lists the thickness values.

TABLE 14 - "B" MODEL WALL THICKNESSES

Component	Model 1 length (mm)
Silica (Ls)	60
Adhesive (La)	10
Aluminum (Lm)	6

This model has a heat flow of 31 kW/m^2 and it has a surface temperature of 1006ºC. The final distribution of temperatures is presented in Figure 44. The temperature in the aluminum inner wall is 324.7 ºC

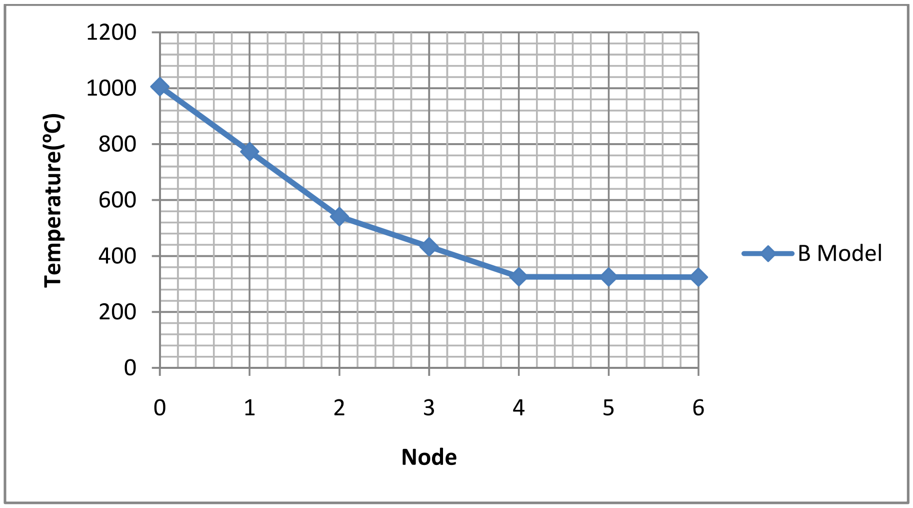

FIGURE 44-TEMPERATURE DISTRIBUTION ALONG THE "B" MODEL

Figure 45 shows the evolution of the adhesive temperature during 10 minutes of heating. The maximum temperature in the adhesive layer is 325ºC.

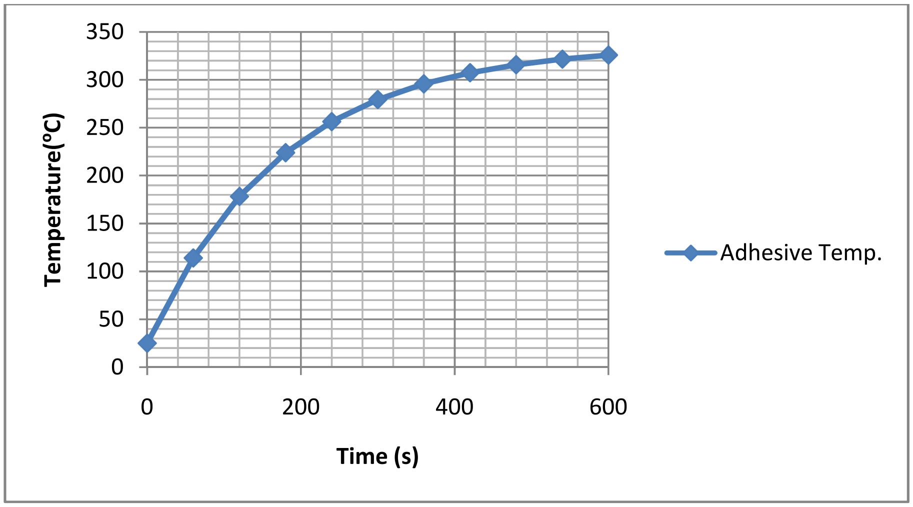

FIGURE 45 -ADHESIVE CORE TEMPERATURE VARIATION WITH TIME

The last model tested is called "C" model. This has keeps the same thickness of the silica tile and aluminum panel of the "B" model, but reduces the adhesive layer to a reasonable 1 mm. The thickness information is summarized in Table 15.

TABLE 15 – "C" MODEL WALL THICKNESSES

Component	Model 1 length (mm)
Silica (Ls)	60
Adhesive (La)	1
Aluminum (Lm)	6

This model has very limited resistance to heat flow, so it is traversed by a power of 39 kW/m^2. The outer wall temperature is 1003 ºC .The final temperature distribution is presented in Figure 46. The temperature in the aluminum inner wall is 397.8 ºC.

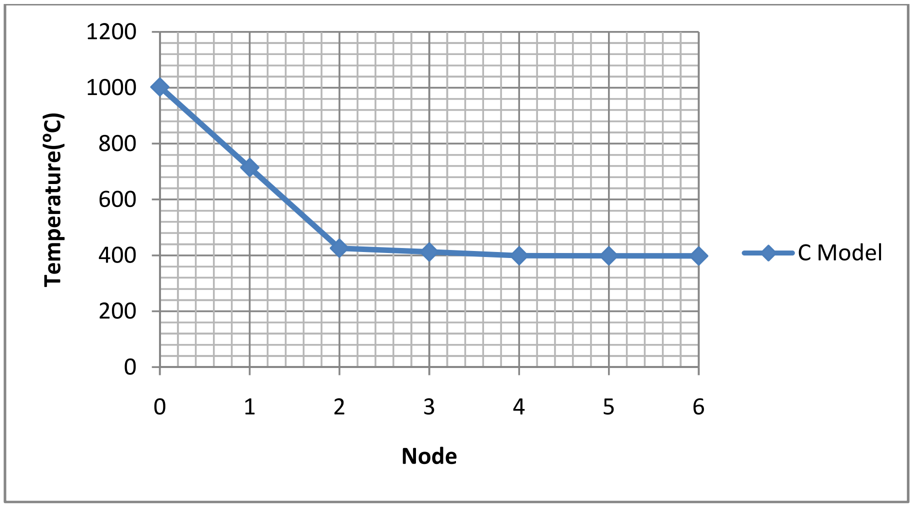

FIGURE 46-TEMPERATURE DISTRIBUTION ALONG THE "C" MODEL

The evolution of adhesive core temperature with time is shown in Figure 47. It shows a maximum temperature of 399ºC in the adhesive core. This temperature is due to the higher heat flow enabled by the smaller walls.

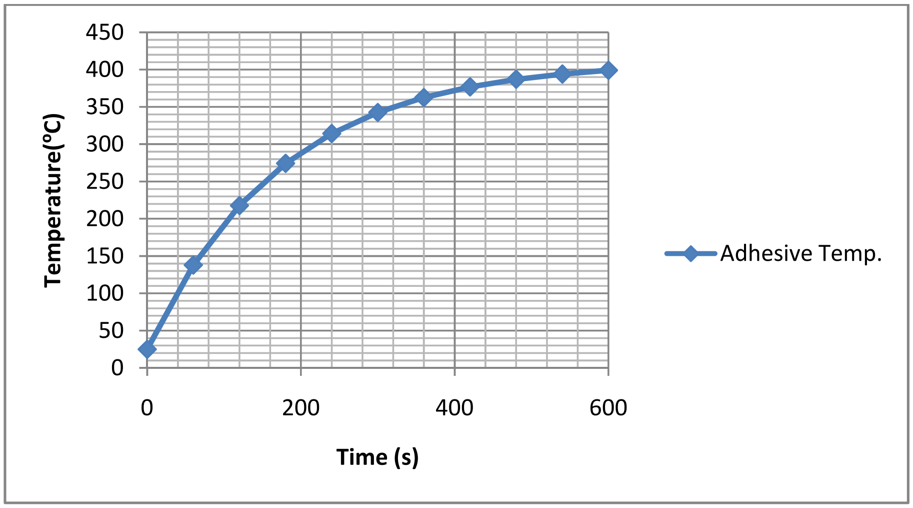

FIGURE 47 -ADHESIVE CORE TEMPERATURE VARIATION WITH TIME

If we analyze the changes to the silica tile thickness made to the adhesive core temperature, as shown in Figure 48 , we can have an indication of the importance of its thickness.

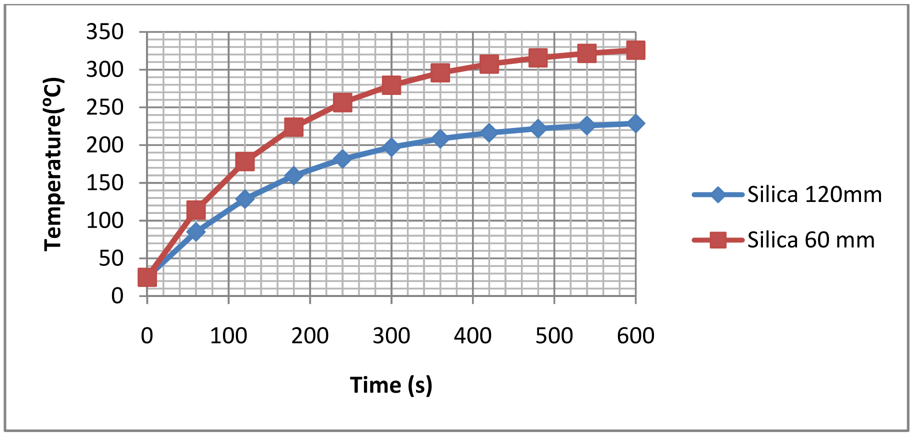

FIGURE 48-ADHESIVE CORE TEMPERATURE EVOLUTION FOR DIFFERENT SILICA TILE THICKNESSES

The use of half of the silica tile thickness results in an increase of the conducted heat power by roughly 25%. The final temperature of the adhesive layer is 42% higher, making the aluminum temperatures jump to excessive values. It is known that the silica tiles used in real applications have thicknesses around 120mm and this is consistent with this analysis.

The ten-fold reduction in the adhesive layer thickness results in the distributions shown in Figure 49.

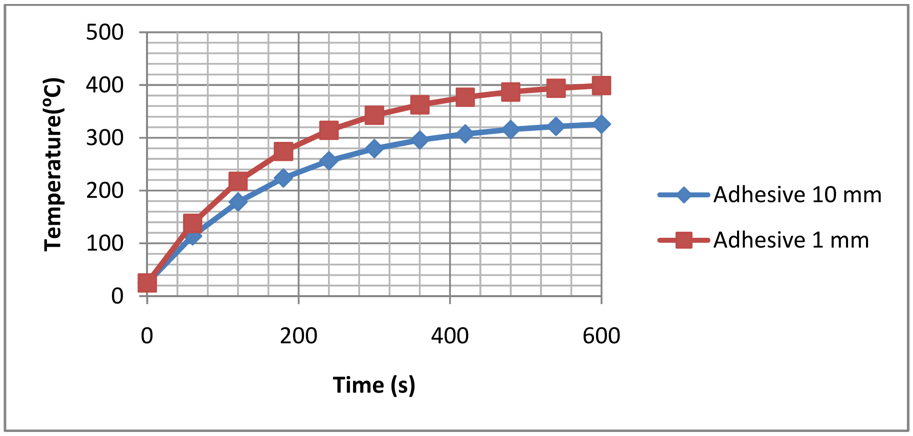

FIGURE 49- ADHESIVE CORE TEMPERATURE EVOLUTION FOR DIFFERENT ADHESIVE LAYER THICKNESSES

The reduction brought a power increase of 25%. We can conclude that in these specific conditions of operation the adhesive layer is 5 times less influential in the power conduction of the heat shield. The absolute values of the aluminum layer temperature are exaggerated by the use of a thin silica tile length, but if we analyze them in relative terms, we find that the final temperatures differ by only 22%. This corroborates the notion that the silica tile is in fact the better place to block the incident heat flow. This notion is further supported by the fact that the silica tiles are less expensive and have less specific weight that the adhesive layer.

If we observe the final temperature distributions for both cases we will also see that most of the temperature is located in the silica tile, and the adhesive layer has a temperature similar to that of the metallic structure. This means that the adhesive is in equilibrium with the aluminum layer and does not store large amounts of energy as the silica tiles do.

Regarding the temperatures encountered, it is safe to say that some organic adhesives would be able to successfully function at the temperatures encountered. The main thermal issue that arises with the utilization of a ceramic adhesive is the fact that ceramics are only necessary if thin silica tiles are employed, which leads to excessive temperatures at the adhesive layer that end up passing to the vehicle structure. The use of a ceramic adhesive layer might require a radically different heat shield structure where its undeniable advantages might be successfully employed.

5.2 DUAL ADHESIVE JOINT SIMULATION

The main objective of the dual adhesive joint simulation is to determine the stress distributions in the joint for a better understanding of the load transfer and joint strength optimization. Elastic and plastic analyses were performed.

Elastic analysis can give a first view of the stress distribution in the adhesive when taper angles and dual adhesives are used – However, for joint strength prediction and comparison with the experimental load displacement curves, a plastic analysis is a necessity.

The adhesive yielding can be modeled using the von Mises criterion; however, the most accurate models for polymers are those that take into account the hydrostatic stresses such as the Drucker and Prager

The model of Drucker-Prager can be expressed in the following equation:

$$aq^b - p = p_t \tag{7}$$

The terms of this equation are defined as:

$$a = \frac{1}{3(\lambda-1)\sigma_t} \tag{8}$$

$$q = \sqrt{\frac{1}{2}[(\sigma_1-\sigma_2)^2+(\sigma_2-\sigma_3)^2+(\sigma_3-\sigma_1)^2]} = \sqrt{3J_2} \tag{9}$$

$$b = 2 \tag{10}$$

$$p = -\frac{1}{3}(\sigma_1+\sigma_2+\sigma_3) = -\frac{1}{3}I_1 \tag{11}$$

$$p_t = \frac{\lambda\sigma_{yt}}{3(\lambda-1)} \tag{12}$$

The exponential Drucker-Prager criterion is implemented in ABAQUS version 6.6-3, the software program used to perform this study. It requires three parameters: a, b and dilation angle.

The model of Drucker-Prager requires data from compression and tensile testing to calculate the S ratio. According to Karachalios, Adams (24) an alternative method can be used to enable calculation with tensile and shear test results. These are the tests that were performed during the course of this work, so this technique is very appropriate for this case. To find the parameters that correctly model the adhesive, a comparative method is needed.

Comparisons were performed between finite element analysis models and actual test results. Finite element models loaded with tensile test data were subjected to a pure shear stress load (depicted in Figure 50), from which one can obtain a shear stress-strain distribution. By varying the parameters of the variables in the Drucker-Prager criterion, one can obtain a series of shear stress-strain distributions and compare them with the actual experimental TAST test results.

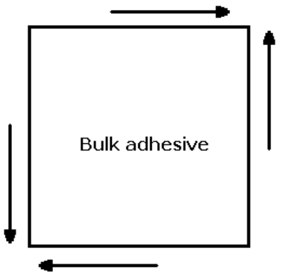

FIGURE 50-- PURE SHEAR STRESS MODEL

The comparison was done by fixing the variable *a* and *b* finding a dilation angle that allows a matching between the simulated and real TAST curves.

The procedure is described here for the adhesive Araldite 2015.

We started by choosing an initial *a* value, selected from experience with other similar adhesives. This derives from the use of a ratio of 1.4 between the yield stress in tension and compression. The initial *b* value of 2 was imposed by the exponential form of the equation.

- a=0,041 (λ =1,4)
- b= 2

The Drucker-Prager model imposes a limit in the dilation angle. The value of the dilation angle must not be higher than the value of the angle of internal friction according to the software documentation.

$$sin(\phi) = \frac{3(\xi-1)}{3\zeta+1} \qquad (13)$$

The value of the angle of internal friction is 13 degrees. This means that the dilation angle is limited between 0 and 13 degrees.

The Drucker-Prager model implemented in ABAQUS also requires strain hardening information to be introduced. This information can come from two different sources: tensile testing and shear testing. As we were performing a shear test in ABAQUS, we chose to introduce the plasticity data information obtained in tensile testing.

The maximum value of the dilation angle was used to run the TAST simulation in ABAQUS and then compared with the actual test result. The curves, shown in Figure 51, are very closely matched.

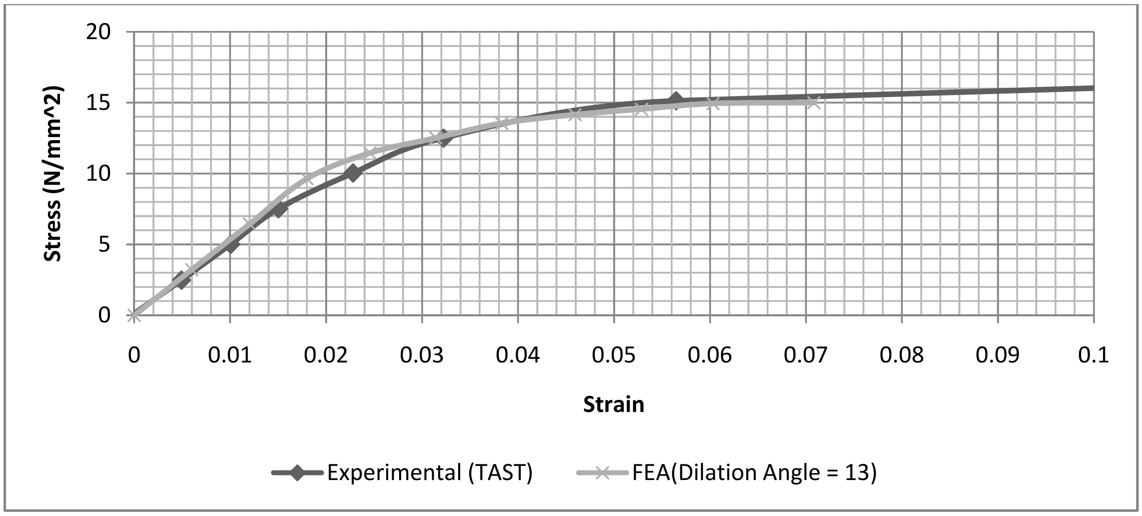

FIGURE 51 - SHEAR STRESS DISTRIBUTION COMPARISON (TAST AND SIMULATED TAST WITH DRUCKER-PRAGER)

The model shows a remarkable similarity with the experimental results obtained from TAST experimental procedures. There is only a small deviation in the plastic portion of the curve and at the end of the graph. These differences are very small though, and take nothing away from the model usefulness. All the remaining parameters (*a* and *b*) were kept, as there is no need to further modify the curve. Table 16 lists these relevant parameters.

TABLE 16-DRUCKER-PRAGER PARAMETERS FOR ARALDITE 2015

Parameter	***Value***
a	0,041
b	2
Dilation angle	13º

Another adhesive studied in this work is the Araldite AV138/HV998 combination. The exponential parameters for this adhesive were gathered from literature and are listed in Table 17 (14).

TABLE 17- DRUCKER-PRAGER PARAMETERS FOR ARALDITE AV138

Parameter	*Value*
a	0,03045
b	2
Dilation angle	20º

To complete the Drucker Prager model more data describing the plastic behavior of the adhesive in tensile testing is required. This data is obtained by considering the plastic portion of the stress-strain curve, and calculating the plastic strain for some stress values. These points are used to construct plastic models for the adhesives.

The plastic strain is calculated by removing the elastic component from the total strain. This is accomplished by drawing lines that go from the elastic points of the curve to the strain axis, parallel to the elastic portion of the graph. The point where these lines intercept the strain axis is the value of the plastic strain.

Using stress strain-stress curves for each adhesive the data points in Table 18 and Table 19 were obtained.

TABLE 18-PLASTICITY DATA FOR ARALDITE 2015

Stress (MPa)	*Plastic Strain*
15	0
20.2	0.01
22.2	0.0225
22.37	0.038

TABLE 19- PLASTICITY DATA FOR ARALDITE AV138

Stress (MPa)	*Plastic Strain*
36.49	0
40.01	0.0013

The dual adhesive joints were modeled in ABAQUS using the boundary conditions shown in Figure 52.

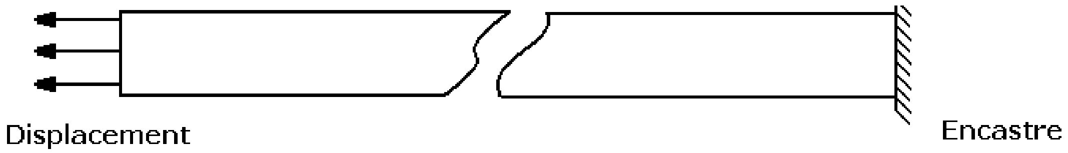

FIGURE 52- FINITE ELEMENT MODEL BOUNDARY CONDITIONS

These boundary conditions were intended to simulate a tensile test, as one of the objective of this work is to obtain direct comparisons between experimental and simulation data. The validation of this data requires that the conditions are as identical as possible.

The displacement applied is 1 mm. This value is more than necessary to break the adhesive connection and in the end of the simulation the entire adhesive layer is plasticized.

The mesh used was composed of CPE8R elements, which are 8-node bi-quadratic plane strain quadrilateral elements, with reduced integration to enable faster calculation. Each element was 0.2 mm long. The mesh and the model were designed using the CAE visual interface of ABAQUS. A general aspect of the mesh can be seen in Figure 53.

This mesh is relatively simple and rough, as it does not use any selective or local refinement. A comparative analysis was made with different meshes of different resolutions. It was found that the stress distributions for this mesh were very similar to those obtained with meshes with the double of the density. For simplicity and faster processing times this mesh was selected.

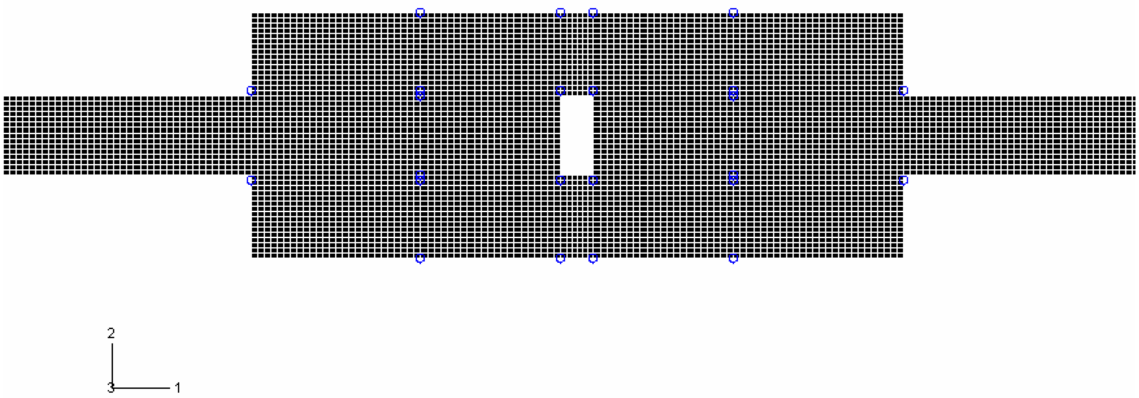

FIGURE 53-FINITE ELEMENT MODEL MESH ASPECT

Node reactions at the encastre section are requested in the model. Node displacements at a distance of 25 mm to the left of the center of the specimen and 25 mm to the right of the center of center are also requested in the model. The displacements of the right node set are subtracted to the displacements of the left node set. The reactions are obtained from this point as this simulates the displacement read by the extensometer with a 50 mm reference length. This calculated displacement is combined with the sum of the node reactions and plotted in an x-y graph to obtain the load-displacement curve. This distribution can be directly compared with the actual tensile test experimental data.

The following graphs show the Von Mises stress equivalent for paths that pass exactly in the center of the adhesive layer (including the tapered area). There is one graph for each adhesive combination, with the various taper angles and their respective stress distributions.

Von Mises equivalent stress was chosen for this analysis as it encompasses all of the different stresses in the different directions acting on the adhesive. A von Mises stress distribution allows a quick and relevant assessment of the stress state in the joint.

To choose the location of the path, a small parametric study was made. Stress distributions for three different locations in 45º tapered patch specimen were obtained in ABAQUS. The adhesive used was Araldite 2015. The path locations are explained in Figure 54. The von Mises stress distributions for each path are represented in Figure 55.

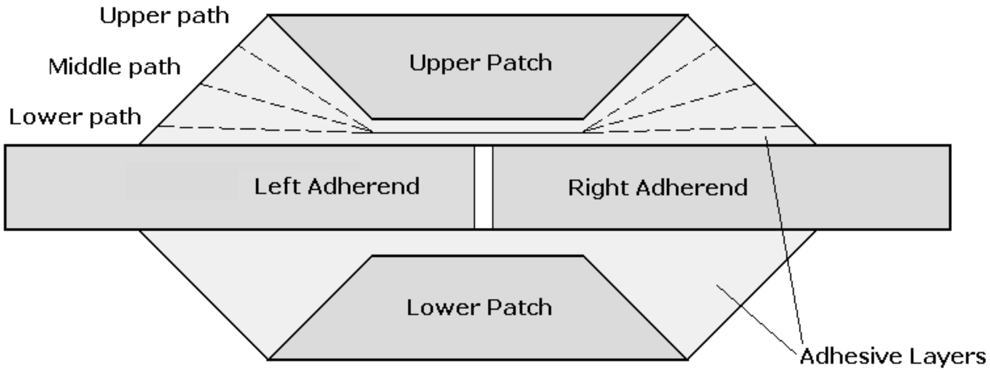

FIGURE 54- PATH LOCATION COMPARISON

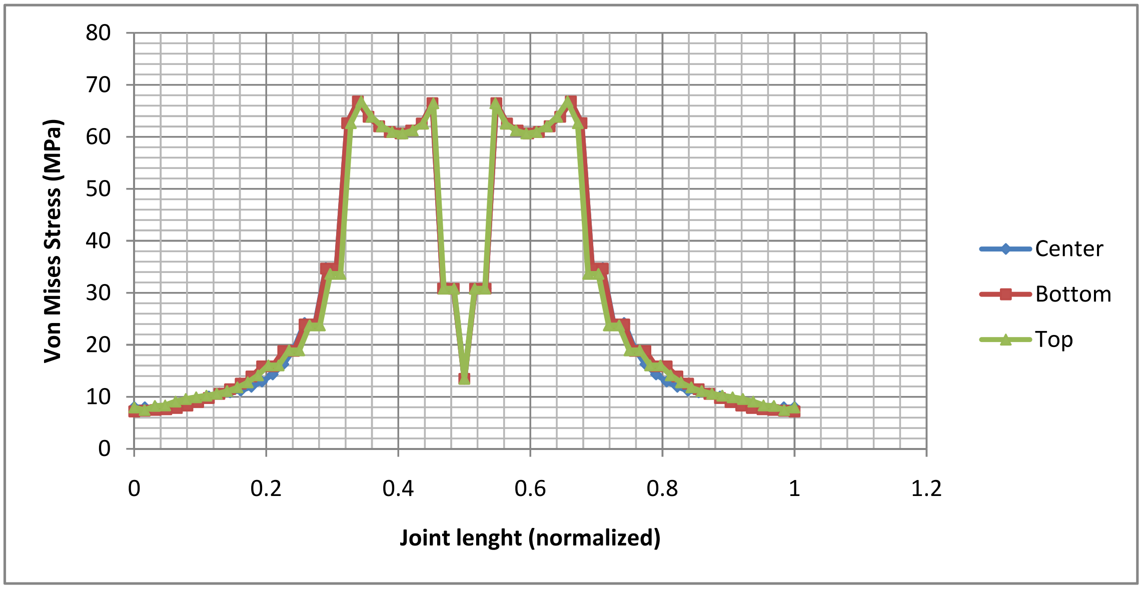

FIGURE 55-VON MISES STRESS FOR DIFFERENT PATH LOCATIONS

This graph shows that the differences are very small for the three locations and in fact there is overlap for the most part of the stress distribution. Based in this data it was decided to use the middle path for simplicity reasons.

The displacement applied for these plastic models was only 0.5 mm to the left in the left extremity. The stress values displayed are, due to the nature of an elastic model, only to be understood as relative and not indicative of actual joint strength.

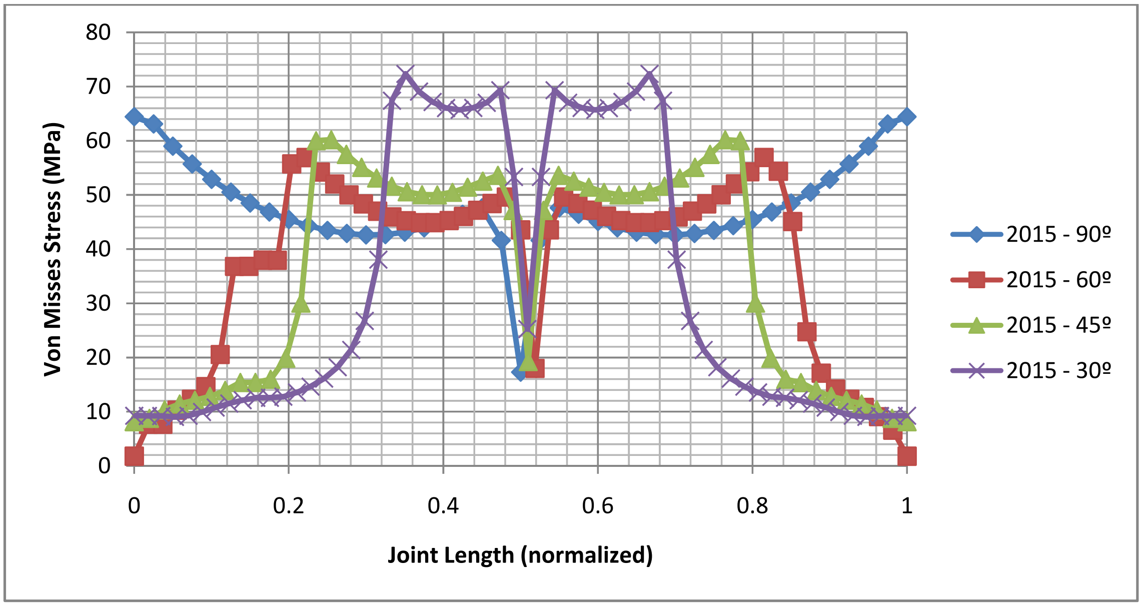

FIGURE 56- VON MISES STRESS DISTRIBUTIONS FOR 2015 ADHESIVE MODELS

Figure 56 shows the von Mises stress distribution for Araldite 2015 adhesive (E= 1850 MPa). It shows that in the absence of a taper angle the stress at the end of the patch are extremely high and concentrated. This is obviously the worst case scenario. The use of taper angles immediately lowers the tip stresses to near zero. As the taper becomes longer and less steep, the loads are transferred to the center section.

Extremely lower taper angles bring excessive stress to the center section and offer lower joint strength. The ideal angles in this configuration are 60° and 45°. They combine smooth stress distribution at the tips with stresses in the center that are close those offered by 90° configuration.

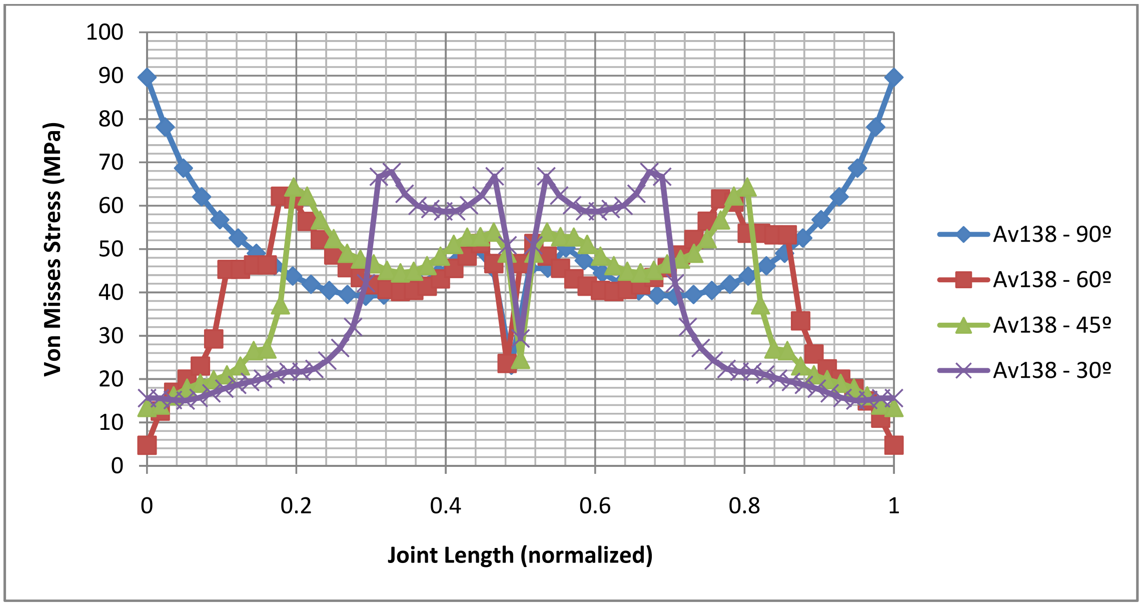

FIGURE 57-VON MISES STRESS DISTRIBUTION FOR AV138 ADHESIVE MODELS

Figure 57 shows the von Mises stress distributions for AV138 (E=4590 MPa). In the case of the 90° the stress at the tip is 40% higher that for the other configurations. This demonstrates that the taper angle is much more useful in stiff adhesives. The optimal taper angles for this case still appear to be the 45° and 60° configurations which are very closely matched and similar. It is interesting to note that at the tip of the taper the stresses for all angles are higher than verified for Araldite 2015.

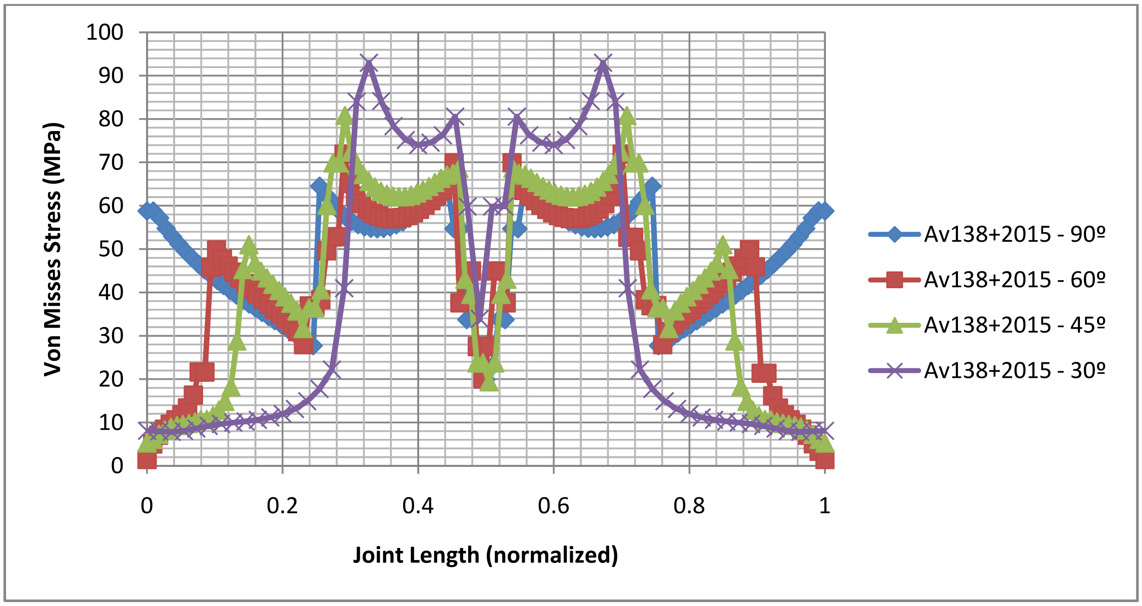

FIGURE 58- VON MISES STRESS DISTRIBUTION FOR DUAL ADHESIVE MODELS

The last case studied, is depicted in Figure 58 and shows the combination of the two adhesives represented in the previous graphs. The stiffer adhesive (Av138) is placed in the center of the joint while 2015 is placed in the taper. This assures lower stresses at the tip, leading to smaller stress concentration. For the 90° taper angle, we see that the tip stress is identical to that verified using 2015 alone, but using a stronger adhesive in the center section will almost certainly result in a stronger joint. This fact, among others in the graph, shows that the stress distribution of the adhesive combination is in fact an assembly of the individual distributions of each adhesive. If necessary, a joint can be engineered with specific stress distributions by combining sections of different adhesives and controlling their length.

The plastic model for these joints was to be applied to the taper angles and use the Drucker-Prager criterion to accurately represent the plastic behavior of the adhesive. Unfortunately, the Drucker Prager criterion could no be implemented successfully in time and a simpler Von Mises criterion had to be implemented. This criterion simply requires the plastic stress/plastic strain data points to be implemented in ABAQUS. Those data points are listed in the “Dual Adhesive Joint Simulation” of this work.

Additionally mesh definition problems also plagued the implementation of the plastic model in the tapered angle specimens. These require perfectly structured mesh which could not be implemented with ABAQUS CAE. This mesh is going to be designed manually and implemented in a parametric form so that the implementation of models with different angle is simpler.

Plastic analyses were done only for the 90º models (without taper) – The load displacement curves are presented for each of case in Figure 59, Figure 60 and Figure 61.

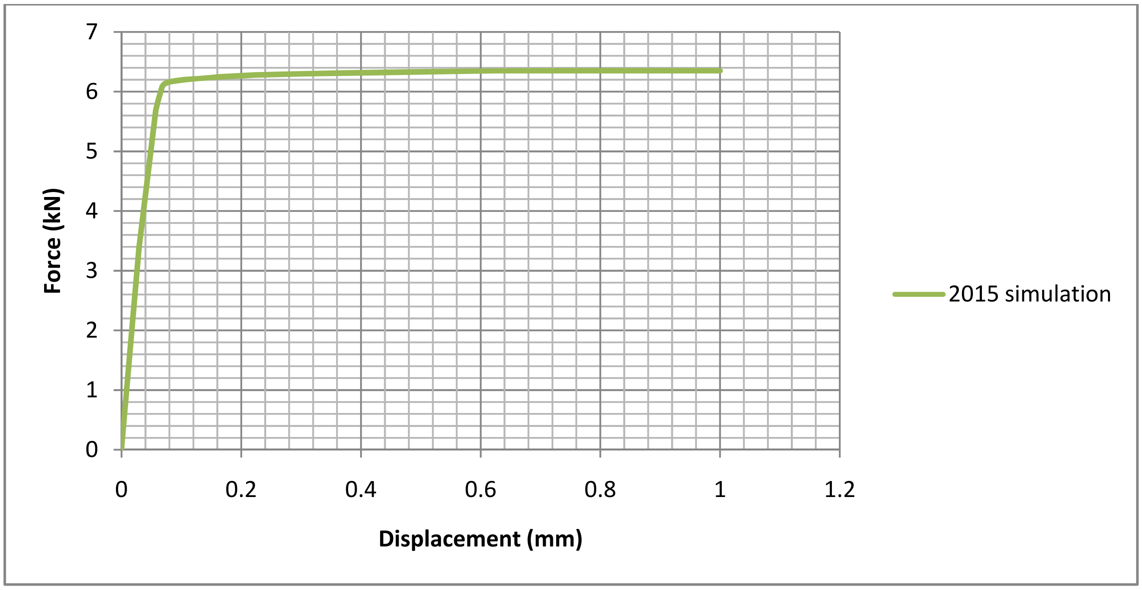

FIGURE 59-FEA LOAD-DISPLACEMENT CURVE FOR 2015 ADHESIVE; 90° PLASTIC MODEL

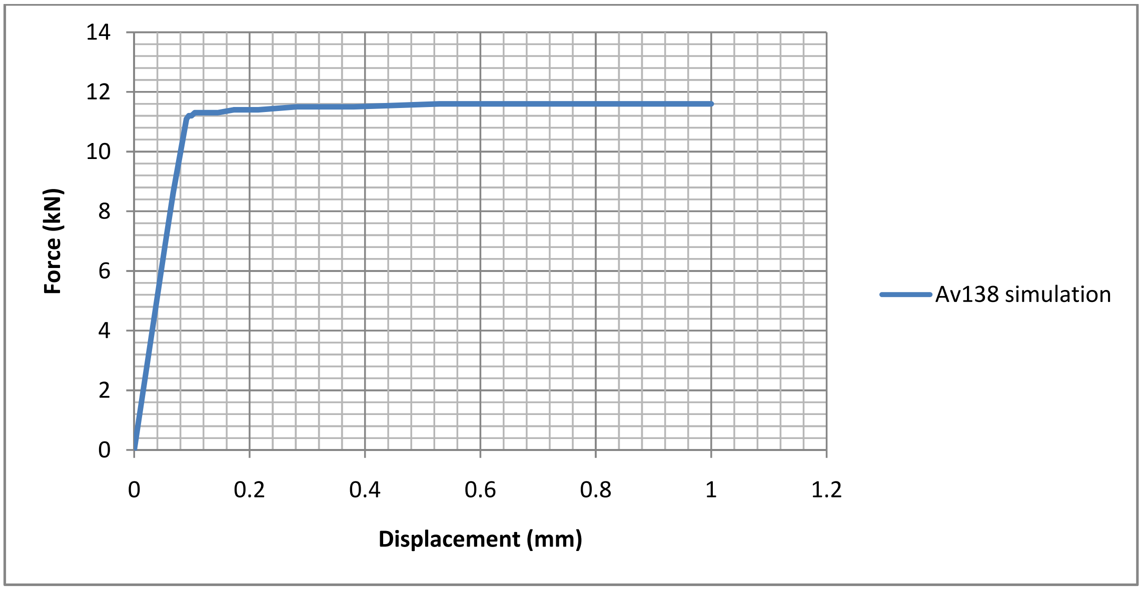

FIGURE 60-FEA LOAD-DISPLACEMENT CURVE FOR AV138 ADHESIVE; 90° PLASTIC MODEL

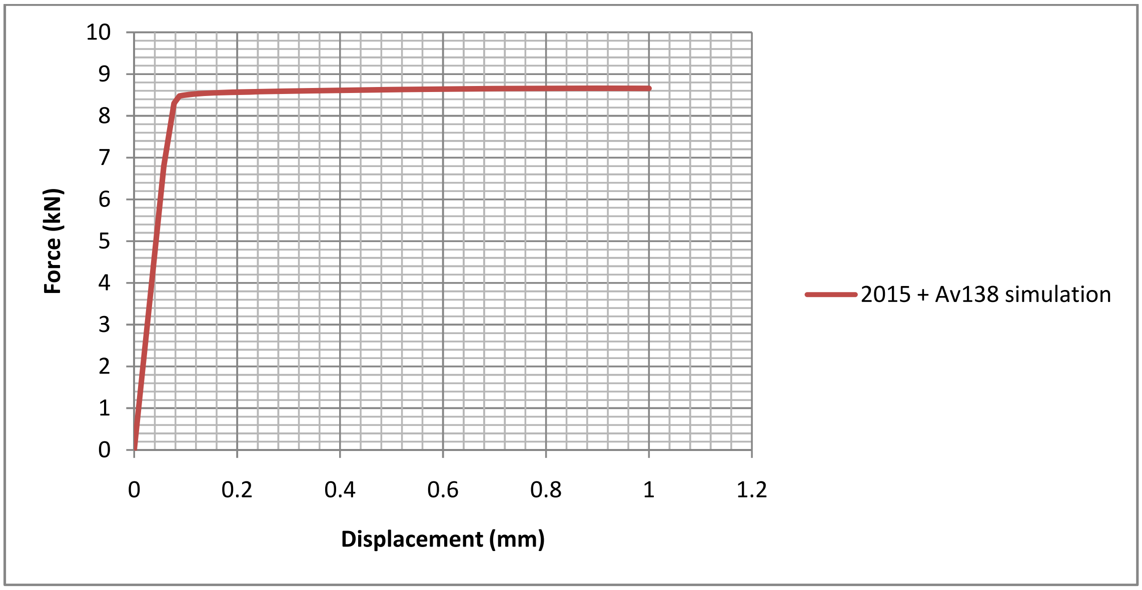

FIGURE 61- FEA LOAD-DISPLACEMENT CURVE FOR 2015+AV138 ADHESIVE COMBINATION; 90° PLASTIC MODEL

5.5 COMPARISON BETWEEN EXPERIMENTAL AND SIMULATION DATA

Data obtained from the plastic simulations can be directly compared with data from tensile tests in the form of the load-displacement curves. In these graphs, the model to predict failure in the FEA load-displacement is simply the consideration that the adhesive joint will fail at the displacement verified in experimental procedures. This is a very simple empirical model that will be used until more precise and detailed plastic simulations are available.

The first of the model comparisons to be made is with the 2015, 90º taper angle model. It is shown in Figure 62.

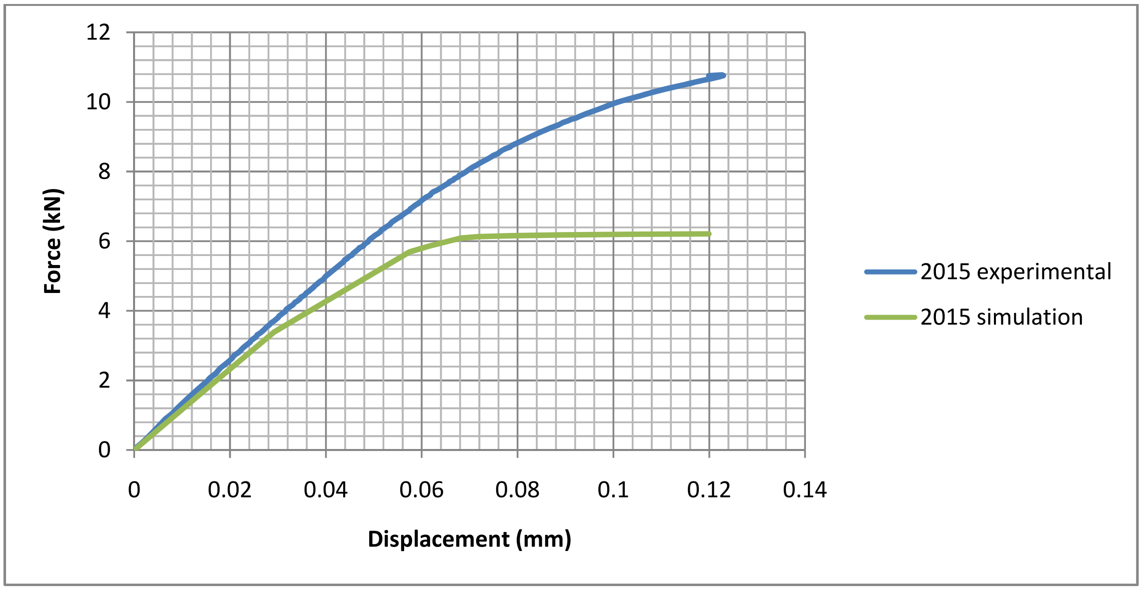

FIGURE 62- COMPARISON OF LOAD-DISPLACEMENT CURVES, 2015 AND 90° TAPER

This model has difficulties in predicting the joint resistance of the joint. Despite matching quite well the displacement curve of the experimental data it plasticizes too early, resulting in a maximum force of 72% less than the practical data. The mechanical properties of Araldite 2015 are most likely causing this offset.

The second comparison is made with the AV138, 90º taper angle model. This comparison is shown in Figure 63.

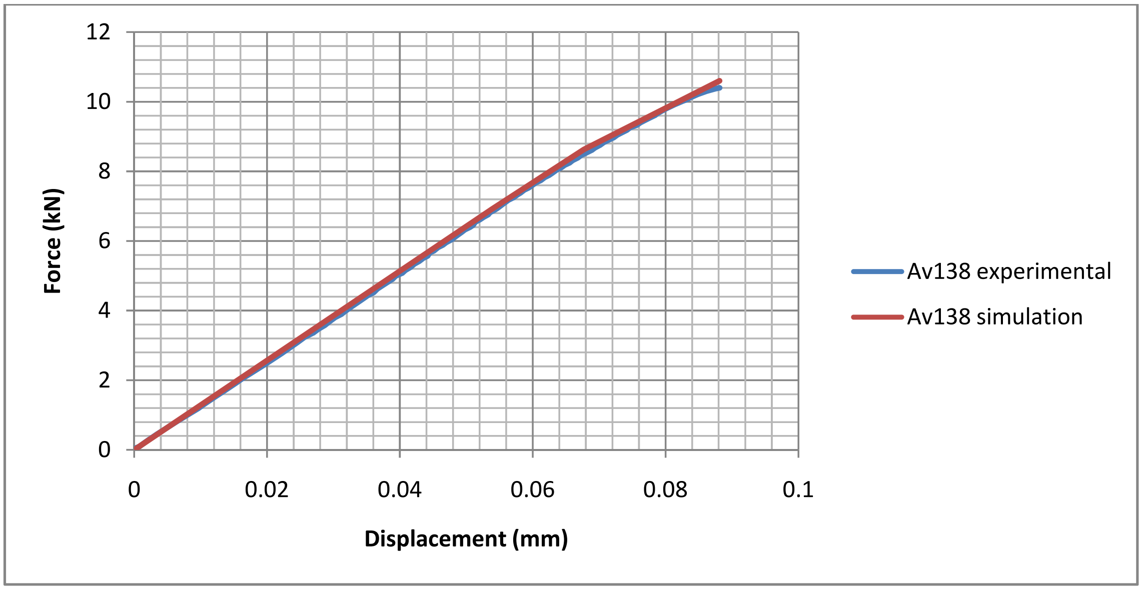

FIGURE 63- COMPARISON OF LOAD DISPLACEMENT CURVES, AV138 AND 90 ° TAPER

In this case an almost exact match of curves is obtained. The predicted value is only 1.9% different from the experimental value. This model can be considered an accurate representation of the real joint under plastic conditions.

The final model to be compared is the 2015+AV138 90º taper angle model, depicted in Figure 64.

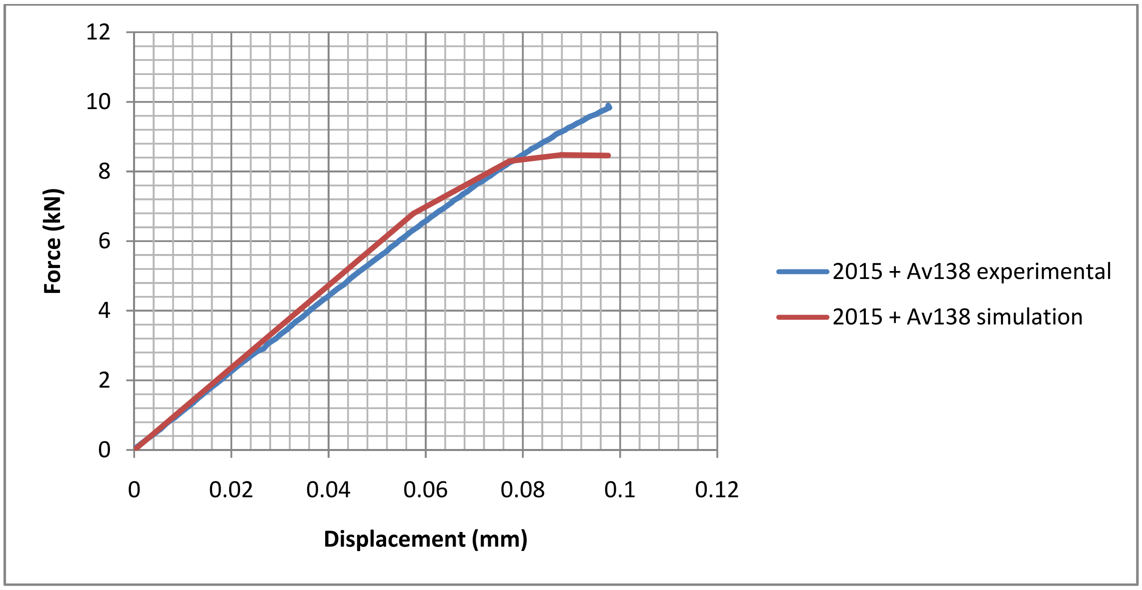

FIGURE 64- COMPARISON OF LOAD DISPLACEMENT CURVES, 2015+AV138 AND 90º TAPER

This simulated model is much better approximated to the experimental data, and models the displacement very accurately for the most part of the curve. In the final section, there is a deviation, probably caused by the same reason that produced the discrepancy in the load displacement curve of the Araldite 2015 adhesive. The model failure load is 17% less than the experimental load, which although not unsatisfactory could be better. The next plastic models to be produced will definitively require corrected mechanical properties for the 2015 adhesive. The geometry and boundary conditions of the problem seem to be correct as the result obtained with Av138 appears to indicate that.

6. CONCLUSIONS AND FUTURE WORK

The initial characterization tests with ceramic adhesives demonstrated that they are extremely brittle, difficult to handle and to produce joints with. The typical techniques used to characterize adhesives are not useful in this case. To manufacture specimens, special techniques adequate to ceramic materials must be adopted. The mixing and curing procedure must also be reviewed. Consultation with manufacturer is also necessary to identify the limits of the adhesive and determine if it is really the most appropriate material of their catalogue for this specific application

Experimentation with transient heat transmission and temperature gradients demonstrated that for the most common aerospace configuration the maximum temperature that the ceramic adhesive layers encounter is only slightly below 300ºC. This is a relatively low temperature for a ceramic adhesive and there are some polymeric adhesives able to withstand these temperatures. It is therefore reasonable to question the usefulness of a ceramic adhesive for this application, at least in the studied configuration. A ceramic adhesive must be placed closer to the heat source to be effective.

Still in the theme of heat shielding and heat conduction, it was found that the adhesive layer while able to block heat is not very effective at that, and it might be preferable to use silica tiles or similar to enhance the heat blocking capability. Despite being a ceramic, the adhesive has relatively high density and this turns it into a reasonable heat conductor.

Regarding the combination of adhesives, the stress distributions along the adhesive layer demonstrated that the 90º taper angle configuration has exaggeratedly stresses at the ends of the patch. In contrast, the 30º taper angle configuration has low stresses at the tips, but high stresses in the center section. The stresses for both cases are higher for stiffer adhesives.

Analyzing the stress distributions, the ideal angle is between 60º and 45º, as these values provide a balance between the stresses at the tip and the stresses in the center sections. It was also found that the stress distributions of adhesive combinations are very similar to those of single adhesive joints in the parts which have the same adhesive. The distributions can be engineered to have specific stress distributions if the adhesive properties are well known.

Experimental data shows that rigid materials are those that have the most to gain from the use of tapered patch angles. These adhesives are stronger but more fragile, and therefore more susceptible to the existence of stress risers. The taper angles reduce the stress levels at the tips were they are usually higher. Very ductile materials do not need the tapered patches as they already possess the ability to accommodate high localized stresses without fracturing.

Testing has also demonstrated that for these rigid adhesives a 45º taper angle provides the best improvement of joint strength, which can be as high as 30%. Other values such as 60º and 30º also offer improved resistance but not as high.

Experimental data has also shown that the combination of very rigid adhesive with a more ductile adhesive can have a synergetic effect when there is no taper angle. The existence of a more ductile adhesive in the tip of the joint has an effect comparable to the introduction of a taper angle. In this case the more ductile adhesive accommodates the elevated stresses and delays the failure. The whole system is stronger that each of the adhesives alone because only a small amount of ductile adhesive is enough to handle the stress concentrations.

Relatively accurate modeling of the dual adhesive, 90º taper, plastic model was achieved, the values of the force at failure and the displacement at failure were predicted within acceptable error margins. Further work is still required in the single adhesive models and in the other taper angle models.

7. REFERENCES AND BIBLIOGRAPHY

1. **Lucas F. M. da Silva, R. D. Adams.** Joint strenght predictions for adhesive joints to be used over a wide temperature range. *Internation Journal of Adhesion & Adhesives.* 2007, Vol. 27, pp. 362-379.

2. **Lucas F. M. da Silva, R.D. Adams.** Adhesive joints at high and low temperatures using similar and dissimilar adherends and dual adhesives. *International Journal of Adhesion & Adhesives.* 2007, Vol. 27, pp. 216-226.

3. **Jigang Wang, Quangui Guo, Lang Liu, Jinren Song.** The preparation and performance of high-temperature adhesives for graphite bonding. *International Journal of Adhesion & Adhesives.* 2005, Vol. 25, pp. 495-501.

4. **Y, Baziard, R. El Abdi, D. Amara, J.A. Petit.** Study of critical failure parameters for an adhesive-bonded single lap joint with ceramic adherends. *Int. J. Adhesion and Adhesives.* 15, 1995, pp. 155-160.

5. **Rongjun Xie, Liping Huang, Xiren Fu, Yuan Chen.** Effects of Adhesive Composition on Bond Strength of Joined Silicon Nitride Ceramics. *Journal of the European Ceramic Society.* 18, 1998, pp. 901-905.

6. **T.Hong, J. R. Smith. and D.J. Srolovitz.** Theory of Metal-Ceramic Adhesion. *Acta metall.mater.* 7, 1995, Vol. 43, pp. 2721-2730.

7. **Bhowmik, S.** Durabilty of adhesive bonding of titanium in radiation and aerospace environments. 2005, Vol. 26, pp. 400-405.

8. **E. G. Buburaj, D. Starikov, J. Evans, G.A. Shafeev, A. Bensaoula.** Enhancement of adhesive joint strenght by laser surface modification. *International Journal of Adhesion & Adhesives.* 2006, Vol. 27, pp. 268-276.

9. **H.C. Man, X. M. Zhang, T.M: Yue, W.S. Lau.** Excimer laser surface modification of engineering ceramics for adhesive bonding. *Journal of Materials Processing Technology.* 1997, Vol. 66, pp. 123-129.

10. **G.W. Critchlow, C.A. Cottam, D.M. Brewis and D.C. Emmony.** Further studies into the effectiveness of CO2-laser treatment of metals for adhesive bonding. *International Journal of Adhesion and Adhesives.* 1997, Vol. 17, pp. 143-150.

11. **D.R. Halfpenny, D.M. Kane, R.N. Lamb and B. Gong.** Creation of adhesion resistant silica glass surfaces with ultraviolet laser cleaning.

12. **X.M. Zhang, T.M. Yue, H.C. Man.** Enhancement of ceramic-to-metal adhesive bonding by excimer laser surface treatment. *Material Letters.* 1997, Vol. 30.

13. **X.Y Kou, S.T. Tan.** A systematic approach for Integrated Computer-Aided Design and Finite Element Analysis of Functionally Graded Material objectes. 2006, pp. 2549-2565.

14.**da Silva, Lucas F. M., Rodrigues, T. N. S. S. , M. A. V.Figueiredo, M. F. S. M. de Moura, J. A. G. Chousal.** Effect of adhesive type and thickness on the lap shear strength. *Journal of Adhesion.* 82, 2006, Vol. 82.

15. **Lee, Deok-Bo, et al.** Effect of Bond Thickness on the Fracture Toughness of Adhesive Joints. *Journal of Engineering Materials and Technology.* 2004, Vol. 126, pp. 14-18.

16. **J.R.G., Evans.** Direct inkjet printing of ceramics: experiment in teleology. *British Ceramic Transactions.* 2001, Vol. 100, pp. 124-128.

17. **Nasa Kennedy Space Center.** NSTS 1988 News Reference Manual. *www.nasa.gov.* [Online] 1988. http://science.ksc.nasa.gov/shuttle/technology/sts-newsref/stsref-toc.html#sts-tps.

18. Space Shuttle Orbiter Systems. *Science.ksc.nasa.gov.* [Online] http://science.ksc.nasa.gov/shuttle/technology/sts-newsref/sts-tps.html.

19. **Brewer, William D.** Alloys and coating devellopment for metallic TPS for reusable launch vehicles. *www.techreports.larc.nasa.gov.* [Online] 2000. http://techreports.larc.nasa.gov/ltrs/PDF/2000/mtg/NASA-2000-nsmms-wdb.pdf.

20. **K. Keller, J. Antonenko, K.H. Weber.** High-Temperature insulations. *esa.int.* [Online] http://www.esa.int/esapub/bulletin/bullet80/keller80.htm.

21.**da Silva, Lucas F. M., Adams, R. D. and Gibbs, M.** Manufacture of adhesive joins and bulk specimens with high temperature adhesives. *International Journal of Adhesion and Adhesives.* 2004, Vol. 24.

22.**da Silva, Lucas F. M., R. D. Adams.** Techniques to reduce peel stresses in adhesive joints with composites. *International Journal of Adhesion and Adhesives.* 2006, Vol. 27, pp. 227-235.

23. **R. D. S G. Campilho, M. F. S. M. de Moura, J. J. M. S. Domingues.** Modelling single and double lap repairs in composite materials. *Composite Science and Technology.* Article in press, 2005.

24. **E. F. Karachalios, R. D. Adams.** Stress and failure analysis of the single lap joint loaded in tension (theory and experiment). *Submitted for publication.* 2007.

25. **da Silva, Lucas F. M., Magalhães, António G. de and de Moura, Marcelo F. S. M..** *Juntas Adesivas Estruturais.* Porto : Publindústria, 2007.

A. ANNEX

Experimental Strain-Stress distributions

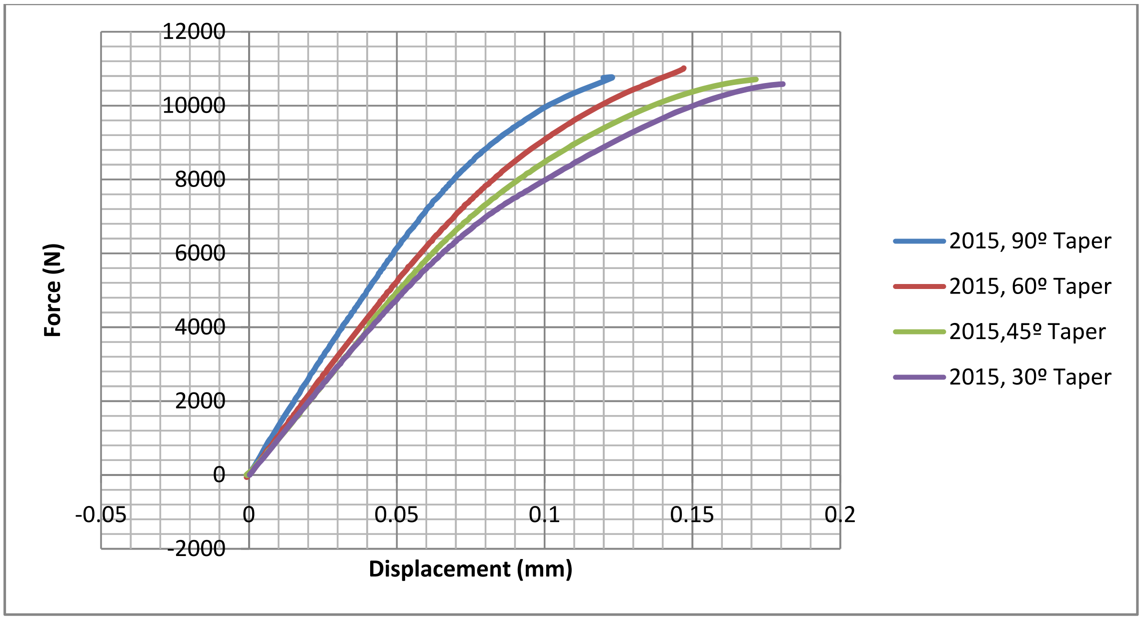

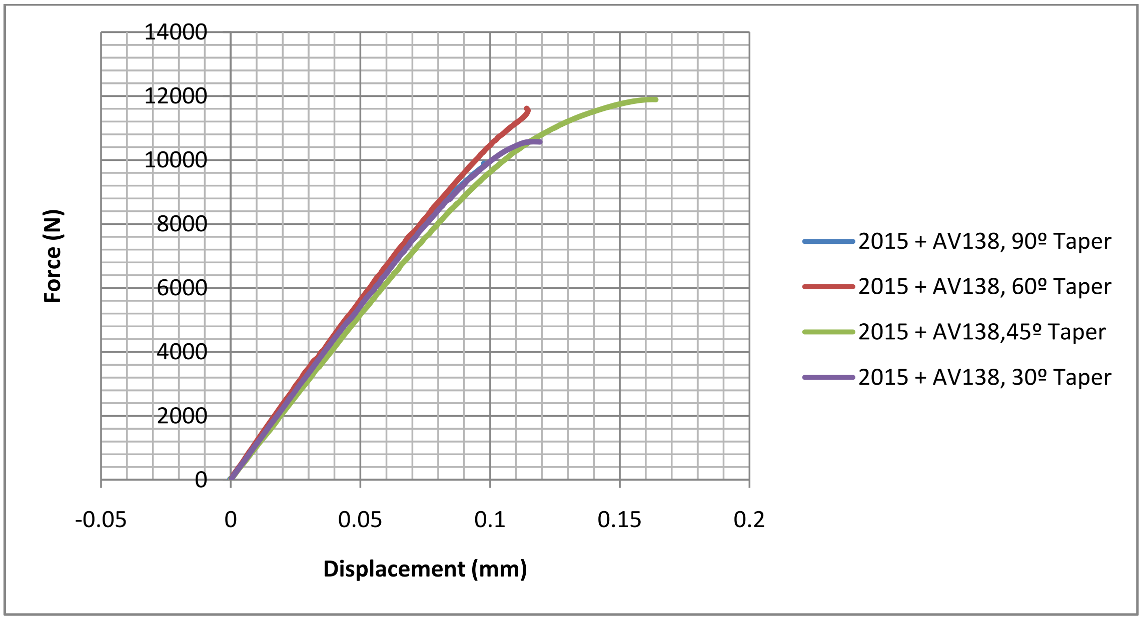

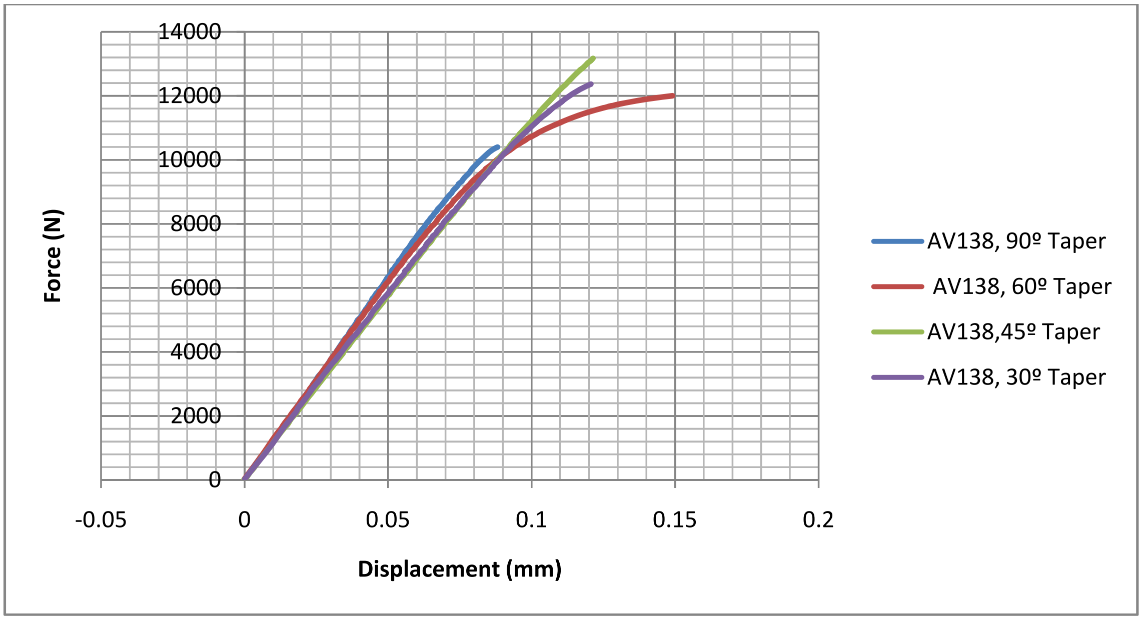
14000
12000
10000
8000
6000
4000
2000
0
-0.05
0
0.05
0.1
0.15
0.2
Force (N)
Displacement (mm)
AV138, 90º Taper
AV138, 60º Taper
AV138,45º Taper
AV138, 30º Taper

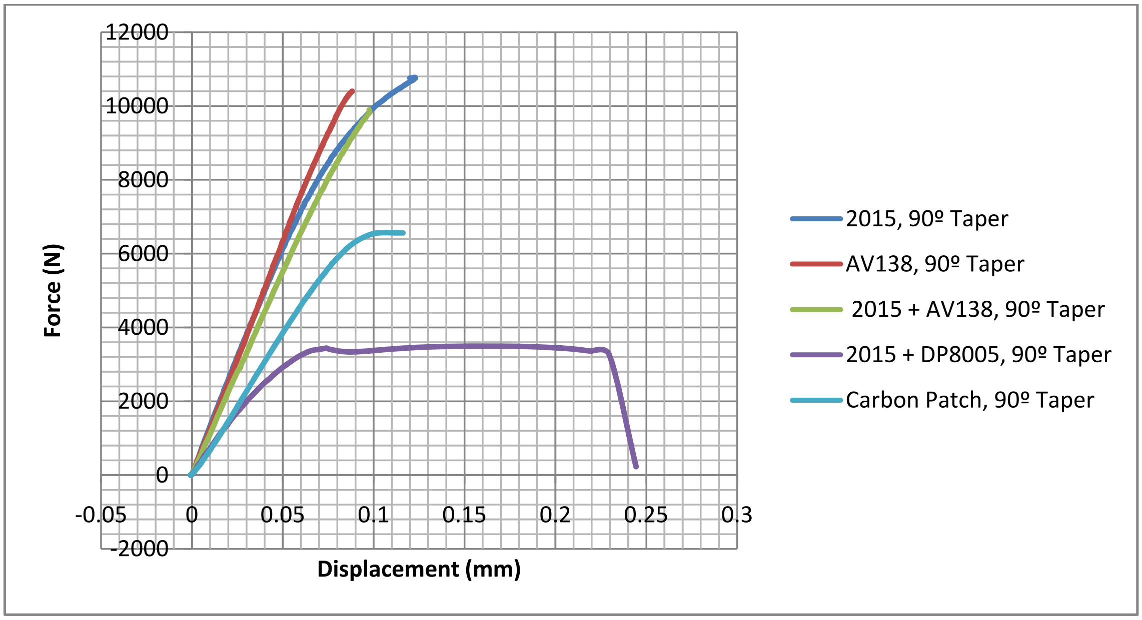
12000
10000
8000
6000
4000
2000
0
-2000
-0.05
0
0.05
0.1
0.15
0.2
0.25
0.3
Force (N)
Displacement (mm)
2015, 90º Taper
AV138, 90º Taper
2015 + AV138, 90º Taper
2015 + DP8005, 90º Taper
Carbon Patch, 90º Taper

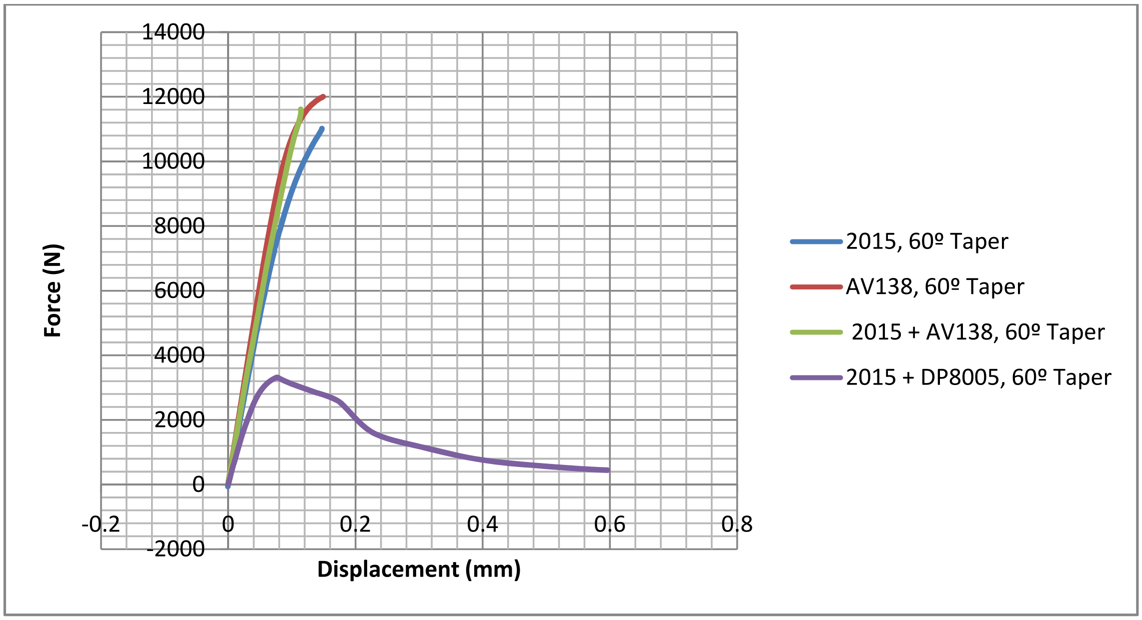
14000
12000
10000
8000
6000
4000
2000
0
-2000
-0.2
0
0.2
0.4
0.6
0.8
Force (N)
Displacement (mm)
2015, 60º Taper
AV138, 60º Taper
2015 + AV138, 60º Taper
2015 + DP8005, 60º Taper

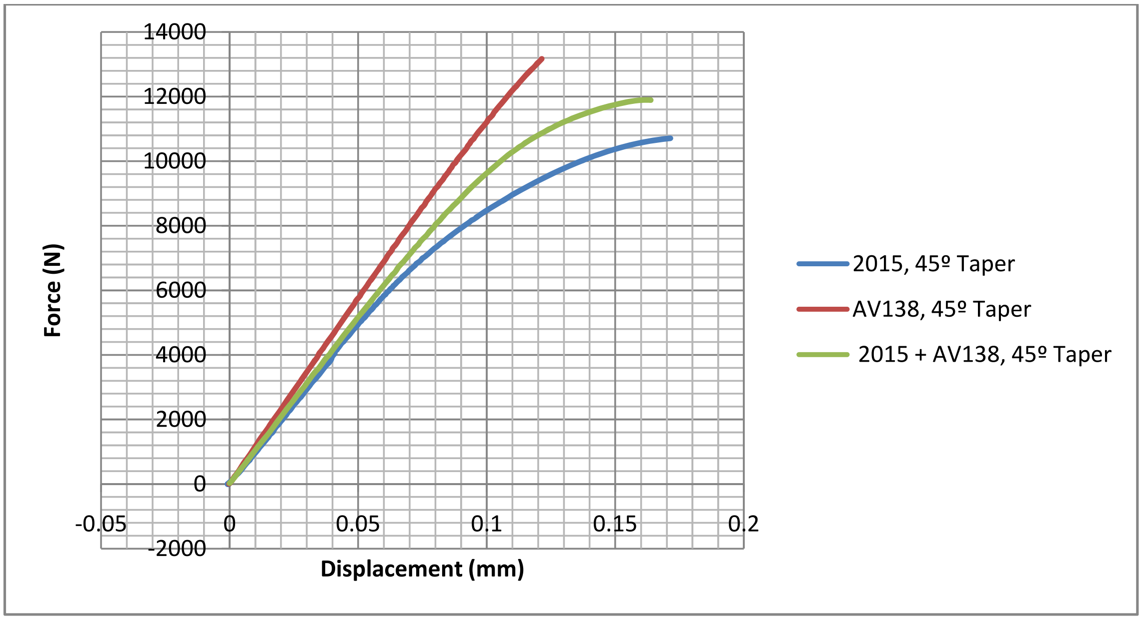
14000
12000
10000
8000
6000
4000
2000
0
-2000
-0.05
0
0.05
0.1
0.15
0.2
Force (N)
Displacement (mm)
2015, 45º Taper
AV138, 45º Taper
2015 + AV138, 45º Taper

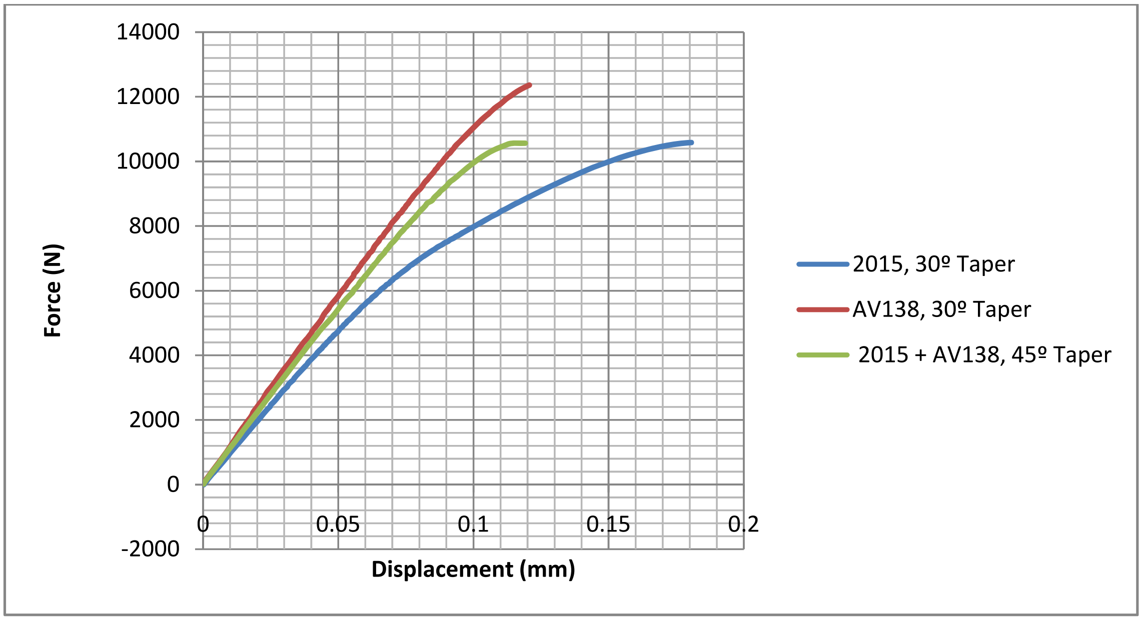
14000
12000
10000
8000
6000
4000
2000
0
-2000
Force (N)
0
0.05
0.1
0.15
0.2
Displacement (mm)
2015, 30º Taper
AV138, 30º Taper
2015 + AV138, 45º Taper

B. ANNEX

EES Thermal Simulation Code

```
"Data"

"Insulating tiles - Silica"
K_si=4 "W/mK"
rho_si=144 "kg/m3"
cp_si=0,84 "J/kg.K"

"Adhesive"
K_ad=1,44 "W/mK"
rho_ad=2000 "Kg/m3"
cp_ad=10 "J/kg.K"

"Aluminium"
K_al=177 "W/mK"
rho_al=2700 "kg/m3"
cp_al=896 "J/Kg.K"

q_dot_0=18000 "W/m2"
h=100 "W/m2.K"
T_ar=25 "ºC"

"Implicit Method"
delta_t=60 "s"
linha=1+tempo/delta_t

"Wall Thicknesses (1/2)"
L_si=0,08 "m"
L_ad=0,005 "m"
L_al=0,003 "m"

"Boundary Conditions"

"First  Knot"
q_dot_0+K_si*(T[1]-T[0])/L_si=rho_si*cp_si*L_si/2*(T[0]-TableValue('Table 1';linha-1;#T[0]))/delta_t

"Last Knot"
h*(T_ar-T[6])+k_al*(T[5]-T[6])/L_al=rho_al*cp_al*L_al/2*(T[6]-TableValue('Table 1';linha-1;#T[6]))/delta_t

"Middle Knots"
k_si*(T[0]-T[1])/L_si+k_si*(T[2]-T[1])/L_si=rho_si*cp_si*L_si*(T[1]-TableValue('Table 1';linha-1;#T[1]))/delta_t
k_si*(T[1]-T[2])/L_si+k_ad*(T[3]-T[2])/L_ad=rho_si*cp_si*L_si/2*(T[2]-TableValue('Table 1';linha-1;#T[2]))/delta_t+rho_ad*cp_ad*L_ad/2*(T[2]-TableValue('Table 1';linha-1;#T[2]))/delta_t
k_ad*(T[2]-T[3])/L_ad+k_ad*(T[4]-T[3])/L_ad=rho_ad*cp_ad*L_ad*(T[3]-TableValue('Table 1';linha-1;#T[3]))/delta_t
k_ad*(T[3]-T[4])/L_ad+k_al*(T[5]-T[4])/L_al=rho_ad*cp_ad*L_ad/2*(T[4]-TableValue('Table 1';linha-1;#T[4]))/delta_t+rho_al*cp_al*L_al/2*(T[4]-TableValue('Table 1';linha-1;#T[4]))/delta_t
k_al*(T[4]-T[5])/L_al+k_al*(T[6]-T[5])/L_al=rho_al*cp_al*L_al*(T[5]-TableValue('Table 1';linha-1;#T[5]))/delta_t
```